REANALYSIS OF AMMONIA/AMMONIUM PARTITIONING AND PARTICLE PH PREDICTION FROM THE ATLANTA AEROSOL NUCLEATION AND REAL-TIME CHARACTERIZATION EXPERIMENT (ANARCHE)

A Thesis
Presented to
The Academic Faculty

by

Qi Wang

In Partial Fulfillment
of the Requirements for the Degree
Master of Science in the
School of Earth and Atmospheric Sciences

Georgia Institute of Technology
May 2018

REANALYSIS OF AMMONIA/AMMONIUM PARTITIONING AND PARTICLE PH PREDICTION FROM THE ATLANTA AEROSOL NUCLEATION AND REAL-TIME CHARACTERIZATION EXPERIMENT (ANARCHE)

Approved by:

Dr. Yi Deng, Advisor
School of Earth and Atmospheric Sciences
Georgia Institute of Technology

Dr. Athanasios Nenes
School of Earth and Atmospheric Sciences
Georgia Institute of Technology

Dr. L. Gregory Huey
School of Earth and Atmospheric Sciences
Georgia Institute of Technology

Dr. Yuhang Wang
School of Earth and Atmospheric Sciences
Georgia Institute of Technology

Date Approved: April 26, 2018

ACKNOWLEDGEMENTS

The last two years of Master's study has been a valuable experience to me, not only in acquiring knowledge but also for my personal growth. I would like to express my sincere appreciation to my advisor, Dr. Yi Deng, for his guidance and support on my study, and his help when I was adapting to the new environment.

I would like to thank Dr. L. Gregory Huey for his support on my thesis. I am truly grateful for his guidance, patience, and availability for discussion during the entire thesis-writing process. I would also like to thank Dr. Athanasios Nenes for his insightful advice on pH calculations. I am thankful to Dr. Yuhang Wang for his time to review my thesis.

I would like to thank Dr. Hongyu Guo, who helped me get familiar with the ISORROPIA-II model. Many thanks to Dr. John B. Nowak, Eric S. Edgerton, and Dr. Rodney J. Weber for data support. Special thanks to Dr. Dana Hartley for her help when I had difficulties. Many thanks to all the professors who have taught me. I enjoyed the classes here.

I would like to express my gratitude to the Georgia Institute of Technology and the School of Earth and Atmospheric Sciences, for the great research environment that makes my study go smoothly and possible.

Finally, I thank my friends for the wonderful time we spent together. I am especially grateful to my parents for their love, support and encouragement that give me motivation all the way.

TABLE OF CONTENTS

LIST OF TABLES

LIST OF FIGURES

LIST OF SYMBOLS AND ABBREVIATIONS

Symbols

a_{H^+}	Hydrogen ion activity
Ca	Calcium
Cl^-	Chloride ion
Fe	Iron
H_2O_2	Hydrogen peroxide
H_2SO_4	Sulfuric acid
H^+	Hydronium ion
H^+_{air}	Hydronium ion concentration in μg m^{-3} air
H^+_{aq}	Hydronium ion concentration in particle liquid water (mol L^{-1})
$H^*_{\mathrm{HNO_3}}$	Equilibrium constant of $HNO_3(g) \leftrightarrow NO_3^- + H^+$
$H^*_{\mathrm{NH_3}}$	Equilibrium constant of $NH_3(g) + H^+ \leftrightarrow NH_4^+$
HCl	Hydrochloric acid
HNO_3	Nitric acid
K	Potassium
Mg	Magnesium
Mn	Manganese
n	Number of moles
N	Nitrogen
Na	Sodium
NH_3	Ammonia
NH_4^+	Ammonium ion

NH_4HSO_4	Ammonium bisulfate
NO	Nitric oxide
NO_2	Nitrogen dioxide
NO_3^-	Nitrate ion
NO_x	NO and NO_2
NO_y	Total reactive nitrogen
O_2	Oxygen
O_3	Ozone
P	Phosphorus
R	Universal gas constant
R^2	Coefficient of determination
SO_2	Sulfur dioxide
SO_4^{2-}	Sulfate ion
W_i	Inorganic particle water concentration in μg m^{-3} air
W_o	Organic particle water concentration in μg m^{-3} air
γ_{H^+}	Activity coefficient of hydronium ion
γ_{HNO_3}	Activity coefficient of hydronium ion-nitrate ion pair
$\gamma_{NH_4^+}$	Activity coefficient of ammonium ion
$\gamma_{NH_4NO_3}$	Activity coefficient of ammonium ion-nitrate ion pair
$\gamma_{NO_3^-}$	Activity coefficient of nitrate ion
$\varepsilon(NH_4^+)$	Partitioning fraction of NH_4^+
$\varepsilon(NO_3^-)$	Partitioning fraction of NO_3^-
σ	Standard deviation

Abbreviations

AMS	Aerosol Mass Spectrometer
ANARChE	Aerosol Nucleation and Real-Time Characterization Experiment
CalNex	California Research at the Nexus of Air Quality and Climate Change
CIMS	Chemical Ionization Mass Spectrometry
CMAQ	Community Multiscale Air Quality Model
CTR	Centreville Site
E-AIM	Extended Aerosol Inorganics Model
EST	Eastern Standard Time
GA	Georgia
GIT	Georgia Institute of Technology Site
GT	Georgia Institute of Technology
IEPOX	Isoprene Epoxydiols
ISORROPIA	“Equilibrium” in Greek
JST	Jefferson Street Site
LWC	Liquid Water Content
NOAA	National Oceanic and Atmospheric Administration
PILS	Particle-into-Liquid Sampler
PM1	Particulate Matter with an aerodynamic diameter less than 1 μm
PM2.5	Particulate Matter with an aerodynamic diameter less than 2.5 μm
ppbv	parts per billion by volume
RH	Relative Humidity
SCAPE	Southeastern Center for Air Pollution and Epidemiology
SD	Standard Deviation

SEARCH	Southeastern Aerosol Research and Characterization
SENEX	Southeast Nexus
SOA	Secondary Organic Aerosol
SOAS	Southern Oxidant and Aerosol Study
SVD	Singular Value Decomposition
T	Temperature
TMI	Transition Metal Ion
UV	Ultraviolet
VOC	Volatile Organic Compound
WINTER	Wintertime Investigation of Transport, Emissions, and Reactivity

SUMMARY

Atmospheric particle acidity, which is described by particle pH, has effects on aerosol formation, composition, and toxicity. It also has impacts on ecosystem and climate. During the past 15 years, NO_x and SO_2 emissions in the United States have decreased by approximately 56% and 82%. In the atmosphere, both NO_2 and SO_2 are oxidized to form HNO_3 and H_2SO_4, respectively, which are the most abundant acidic species in aerosol. In this study, data from the Atlanta Aerosol Nucleation and Real-Time Characterization Experiment (ANARChE) in August 2002 are reanalyzed. Fast ammonia and ammonium measurements were carried out in this experiment, which makes it possible to investigate the diurnal cycle of particle pH, and pH time evolution over the past 15 years in urban Atlanta. Fine particle pH is calculated by ISORROPIA-II, a thermodynamic equilibrium model. For comparison, data from the Southeastern Aerosol Research and Characterization study (SEARCH) at the same site in August 2016 are also used for pH calculation. The result is counterintuitive that fine particle pH did not show an increasing trend, but has slightly decreased despite the emission reduction and the decrease in sulfate and nitrate levels. The average fine particle pH from ANARChE is 1.92 ± 0.58 (±SD), with a median of 1.88, while the average pH from SEARCH is 1.68 ± 0.48, with a median of 1.67. The predicted concentrations and partitioning fractions of semivolatile species (NH_3-NH_4^+, HNO_3-NO_3^-) agree with observations. Sensitivity tests were performed to evaluate the effects of measurement uncertainties on model predictions but no significant effects were observed. The small change in pH from 2002 to 2016 could be explained by the decrease in particle liquid water content and the volatilization of NH_4^+. This is supported by the

decrease of observed NH_4^+ partitioning fraction (from 44.6% in ANARChE to 29.5% in SEARCH).

CHAPTER 1. INTRODUCTION

1.1 Atmospheric Particle Acidity

In the natural environment, the acidity of aqueous solutions is one of the most important fundamental thermodynamic parameters that directly controls chemical reactivity (Seinfeld and Pandis, 2016; Stumm and Morgan, 1996). For example, in cloud drops sulfur dioxide (SO_2) through multistep processes can be oxidized to form sulfate (SO_4^{2-}) which is involatile and can increase the mass of atmospheric particulates (Chameides and Davis, 1982; Harris et al., 2013; Hoffmann and Edwards, 1975; Jacob, 1986; Penkett et al., 1979). However, the efficiency of different SO_2 aqueous phase oxidation pathways is a strong function of acidity or pH of the solution. The pH of an aqueous solution such as a cloud drop or atmospheric aerosol particle, is defined as

$$pH = -\log_{10} a_{H^+} \tag{1}$$

where a_{H^+} is the hydrogen ion activity (e.g. Weber et al. (2016)). For cloud droplets, oxidation of SO_2 by hydrogen peroxide (H_2O_2) dominates under acidic conditions (e.g. lower pH). While SO_2 oxidation by ozone (O_3), nitrogen dioxide (NO_2) and oxygen (O_2, catalyzed by Mn(II) and Fe(III)) is more efficient at more basic conditions in cloud drops (e.g. higher pH, Cheng et al. (2016) and Seinfeld and Pandis (2016)).

In more recent years, the pH of atmospheric particles (e.g. aerosol) has been a topic of active research as it impacts aerosol growth, composition, human health, ecosystems and climate (Dockery et al., 1996; Guo et al., 2016; Guo et al., 2017b; Gwynn et al., 2000;

Meskhidze et al., 2003; Stockdale et al., 2016; Surratt et al., 2010). For example, Cheng et al. (2016) calculated sulfate production rates based on typical concentrations under Beijing haze conditions. They showed that a NO_2-mediated pathway dominates when particles are nearly neutralized, while for more acidic particles, transition metal ions (TMIs) catalyzed oxidation becomes the most important. The production of secondary organic aerosol (SOA) is facilitated by the acidic surface of atmospheric particles via acid-catalyzed heterogeneous reactions (Jang et al., 2002). Laboratory studies have demonstrated that SOA yields from isoprene and acrolein (biogenic VOCs) oxidized by O_3 increase in the presence of acidic inorganic seed aerosols (Jang et al., 2002). Acidic seed particles (i.e. containing H_2SO_4) also enhanced SOA yields from α-pinene ozonolysis (Iinuma et al., 2004). SOA yields from aromatic precursors (toluene and 1,3,5-trimethylbenzene) were increased by acidic seeds (H_2SO_4 + NH_4HSO_4) under dark and UV-visible light conditions without NO_x (Cao and Jang, 2007). During the Southeast Nexus (SENEX) campaign, aircraft measurements of plume from Harllee Branch Power Plant, GA showed that particle acidity accounted for part of the increase of heterogeneous reaction rate constant for isoprene epoxydiols (IEPOX) reactive uptake (Xu et al., 2016).

The soluble bioavailable iron (Fe) in acidic sulfate particles can have an indirect climate impact by regulating the productivity of photosynthesis in the ocean (Li et al., 2017). Ocean productivity in many locations is largely controlled by the availability of nutrients such as nitrogen (N), phosphorus (P) and iron (Moore et al., 2013). Transport and deposition of aerosols (e.g. iron or phosphorus containing mineral dust) to the open ocean can be an important source of nutrients. However, in general the iron or phosphorous delivered to the ocean must be soluble in the aqueous phase to be bioavailable to

photosynthetic organisms. Laboratory experiments have shown a significant increase in soluble phosphorus when Saharan soil and dust samples were exposed to an acidic environment (sulfuric acid, pH = 2) for 24 h (Nenes et al., 2011). Longo et al. (2016) examined Saharan dust aerosols collected at sites with different atmospheric transport time, and found the iron solubility and aerosol acidity greater in aged aerosol. The iron acid dissolution hypothesis is further supported by the soluble Fe sulfate found in the acidic sulfate coating of particles collected over the Yellow Sea (Li et al., 2017). The increased soluble Fe deposition, together with natural climate variability, could enhance biological productivity in tropical Pacific Ocean, and account for the decline of O_2 in the oxygen minimum zones (Ito et al., 2016).

1.2 Aerosol pH Estimation Methods

Direct measurement of the pH of atmospheric particles is challenging and hampered by relatively low time resolution (Hennigan et al., 2015; Jang et al., 2008). Therefore, aerosol acidity is often estimated by proxy methods including (1) the ion balance method based on electroneutrality where the H^+ concentration is derived from the difference between anionic and cationic charge, (2) the molar ratio method where the molar ratio equals the total inorganic cation concentration divided by total inorganic anion concentration, (3) thermodynamic equilibrium models, such as ISORROPIA-II (Fountoukis and Nenes, 2007; Nenes et al., 1998) and the Extended Aerosol Inorganics Model (E-AIM) (Clegg et al., 1998; Friese and Ebel, 2010), (4) ammonia phase partitioning where H^+ activity is calculated from the equilibrium NH_4^+ activity and NH_3 partial pressure (Hennigan et al., 2015). Hennigan et al. (2015) compared these four methods and found that particle pH is best estimated by thermodynamic equilibrium models using both gas

and particle-phase data as input, as well as the ammonia phase partitioning method. The ion balance and molar ratio methods do not uniquely correlate with particle pH (Guo et al., 2015).

1.3 Recent Studies on Particle pH

Fine particle pH has been estimated using the thermodynamic equilibrium model ISORROPIA-II in recent studies. During the California Research at the Nexus of Air Quality and Climate Change (CalNex) study in 2010, the predicted summertime pH values of PM1 and PM2.5 (PM1: particulate matter with an aerodynamic diameter less than 1 μm, PM2.5: less than 2.5 μm) from ground measurements in Pasadena, California are 1.9 ± 0.5 and 2.7 ± 0.3, respectively (Guo et al., 2017a). During the Southern Oxidant and Aerosol Study (SOAS) in 2013, the summertime ground-level pH of fine particles at Centreville site (Brent, Alabama) is estimated to be 0.94 ± 0.59 with a median of 0.93 (Guo et al., 2015). The pH of PM1 based on aircraft measurements of one flight over Georgia as part of the SENEX campaign in June and July 2013 is reported as 1.1 ± 0.4 (Guo et al., 2017a; Xu et al., 2016). The average (mainly in the northeastern U.S.) pH of PM1 from the Wintertime Investigation of Transport, Emissions, and Reactivity (WINTER) aircraft study in 2015 is 0.77 ± 0.96 (median of 0.91) (Guo et al., 2016). Hence, acidic fine particles are ubiquitous. Guo et al. (2017b) suggested that even for the high NH_3 levels in Beijing and Xi'an, China (on average ~12.8 μg m^{-3} in Beijing and ~17.3 μg m^{-3} in Xi'an during some polluted periods in winter), the neutralization of fine particles is unlikely. This is supported by the estimated fine particle pH of 4.2 (pH range: 3.0 – 4.9) based on hourly measurements during Beijing wintertime haze episodes in 2015 and 2016 (Liu et al., 2017).

The prediction accuracy of fine particle pH by ISORROPIA-II is confirmed by comparing the predicted and measured concentrations and partitioning fractions of semivolatile species such as NH_3-NH_4^+ and HNO_3-NO_3^-. The predicted and observed values have good agreement in the above-mentioned CalNex, SOAS, SENEX and WINTER studies. For example, in the WINTER study the slopes of HNO_3, NO_3^- and partitioning fraction $\varepsilon(NO_3^-)$ regression lines are 1.02, 0.99 and 1.17 (R^2 of 0.99, 0.96 and 0.70, respectively) with input from aerosol mass spectrometer (AMS) measurements, while using data from particle-into-liquid sampler coupled with ion chromatographs (PILS-IC) and scaled AMS NH_4^+ led to more scatter (R^2 of 0.71 and 0.27 for NO_3^- and $\varepsilon(NO_3^-)$). The discrepancy between model prediction and observation decreased with increasing relative humidity (RH) (Guo et al., 2016).

Aerosol pH has also been estimated by E-AIM. From the output of AIM-II, the average of submicron particle pH at the Pittsburgh EPA Supersite in September 2002 is 2.4 (median of 2.2, 25th percentile of 1.8 and 75th percentile of 2.9, estimated from Figure S6 of Zhang et al. (2007)). Liu et al. (2017) compared the predicted PM2.5 pH from ISORROPIA-II and E-AIM II during Beijing haze episodes and found the mean absolute pH difference was only 0.3 units.

1.4 Motivation and Overview of the Study

The emissions of SO_2 in the United States have significantly decreased under the Clean Air Act (U.S. Environmental Protection Agency, 2017) due to the implementation of SO_2 scrubbing technologies by power plants and the switch of fuel from sulfur-containing coal to natural gas (de Gouw et al., 2014; Srivastava et al., 2001). The particle

sulfate concentration has also decreased correspondingly (Hand et al., 2012). From 2002 to 2016, the national emissions of SO_2 decreased by ~82%, and ~92% for the state of Georgia (GA). The national emissions of NO_x decreased by ~56%, and ~63% for GA (U.S. Environmental Protection Agency, 2017). However, the emissions of NH_3 are relatively stable (U.S. Environmental Protection Agency, 2017). Weber et al. (2016) showed that despite the large decrease of SO_2 emissions, the pH of fine particles (PM2.5) has remained relatively constant at acidic pHs. This is at least somewhat counterintuitive as the reduction of acid precursor gases such as SO_2 and NO_2 might be expected to lead to higher particle pH. Weber et al. (2016) calculated historical summertime (June, July and August) PM2.5 pH at the Centreville site (same site as SOAS) from 1998 to 2013 using ISORROPIA-II in forward mode (i.e. gas + particle phase data). However, only particle-phase data were used as input, which decreased pH systematically by ~1 unit. The average pH during this period is 0.19 and no increasing trend was observed (pH data from http://www.aerosols.eas.gatech.edu/Weber_Nature_Figure_data.xlsx).

To investigate the change in fine particle pH in the past 15 years, this study reanalyzes data from the Atlanta Aerosol Nucleation and Real-Time Characterization Experiment (ANARChE) in August and early September 2002. The experiment took place at Jefferson Street (JST) in Atlanta, GA, which is also a Southeastern Aerosol Research and Characterization study (SEARCH) site (Nowak et al., 2006). High time-resolution ammonia and ammonium measurements were carried out in this experiment. Two chemical ionization mass spectrometry (CIMS) techniques were used to measure gas-phase NH_3 concentrations and the results have good agreement (Nowak et al., 2006). Nowak et al. (2006) compared the NH_3 measurements with predicted concentrations by a

thermodynamic equilibrium model, ISORROPIA (Nenes et al., 1998). The model calculations also agreed well with observations, which suggests that gas and particle phases are in thermodynamic equilibrium on a 7.5 min timescale. The fast and reliable measurements make it possible to investigate the diurnal cycle of particle pH, as well as its time evolution in the past 15 years by comparison to data taken at the same site in August 2016. The description of the ANARChE and SEARCH dataset, pH calculation method, and SO_2, NO and NO_y data processing is provided in Chapter 2. The characteristics of the SO_2, NO, and NO_y concentrations, model calculations, pH time evolution, the correlation between pH and factors such as RH, liquid water content (LWC) and temperature, the change of NH_4^+ and NO_3^- partitioning fractions with pH, model validation and sensitivity tests are presented and discussed in Chapter 3.

CHAPTER 2. METHODS

2.1 pH Calculations

Due to the limitations of direct measurement techniques of particle acidity (Hennigan et al., 2015), ISORROPIA-II, a thermodynamic equilibrium model was used in this study to calculate fine particle pH, ammonia/ammonium and nitric acid/nitrate phase partitioning (Fountoukis and Nenes, 2007; Nenes et al., 1998). The model was run in forward and metastable mode since it provides better pH predictions (the reverse mode is highly sensitive to measurement uncertainties) and the predictions agree better with observations than the stable mode (Guo et al., 2016; Hennigan et al., 2015). In forward mode, the model is constrained by total (gas + aerosol) concentrations of Na^+, NH_3, HNO_3, HCl, H_2SO_4, K^+, Ca^{2+} and Mg^{2+}, relative humidity (RH) and temperature (T) (http://isorropia.eas.gatech.edu). It is assumed that the aerosol is at metastable state with no precipitation of salts and only one supersaturated aqueous phase exists. Given this assumption, data within the 20-95% RH range were considered in previous studies (Guo et al., 2017a; Guo et al., 2016). Due to the nonlinear dependence of liquid water content on RH and the large uncertainty introduced at high RH (Guo et al., 2017a), data at RH > 95% are excluded from this study. There is no lower limit for ANARChE dataset since the minimum measured RH is 25%.

Based on the ISORROPIA-II output, particle pH is calculated by

$$pH = -\log_{10} \gamma_{H^+} H^+_{aq} = -\log_{10} \frac{1000 \gamma_{H^+} H^+_{air}}{W_i + W_o} \cong -\log_{10} \frac{1000 \gamma_{H^+} H^+_{air}}{W_i} \quad (2)$$

where H^+_{air} is the hydronium ion concentration in μg m^{-3} air, H^+_{aq} the hydronium ion concentration in particle liquid water (mol L^{-1}), W_i and W_o the inorganic and organic particle water concentrations in μg m^{-3} air, respectively (Guo et al., 2017a). γ_{H^+}, which is assumed to be 1 (one of the simplifying assumptions made in ISORROPIA-II), is the activity coefficient of hydronium ion. The organic particle water had a minor influence on pH prediction in previous studies. Guo et al. (2015) reported that particle pH considering W_o is 0.15 to 0.23 units higher than not including W_o in SOAS, and W_o increased pH by 0.12 units on average during the CalNex campaign (Guo et al., 2017a). Therefore, in this study, only W_i is considered in pH calculations.

2.2 ANARChE and SEARCH Data

This study focuses on the ANARChE observations from August 15 to 28, 2002. Two CIMS instruments from the National Oceanic and Atmospheric Administration Aeronomy Laboratory (now part of the NOAA Earth System Research Laboratory's Chemical Sciences Division) and Georgia Institute of Technology (GT) were used to measure gas-phase NH_3 concentrations (Nowak et al., 2006). The NH_3 observations of the two CIMS were found to be in good agreement (Nowak et al., 2006). For the calculations in this work, the NH_3 observations from the GT CIMS were used. Fine particle inorganic composition including the concentrations of Na^+, NH_4^+, Ca^{2+}, K^+, Mg^{2+}, SO_4^{2-}, NO_3^-, and Cl^- was measured by the GT particle-into-liquid sampler (PILS) coupled to a dual channel chromatograph (Orsini et al., 2003; Weber et al., 2001).

The ISORROPIA-II model was constrained by particle-phase data (including refractory ions) and gas-phase NH_3 and HNO_3 data. The NH_3 concentration was reported

every 1 min, which was then averaged to the ~7.5 min PILS sampling frequency. The hourly HNO_3 concentration was linearly interpolated to match the PILS sampling frequency. There is no HCl measurement during ANARChE and the input of total HCl is particle chloride itself. It is assumed that all H_2SO_4 is in particle phase.

For comparison, current pH levels in Atlanta were also calculated based on the SEARCH dataset at JST from August 15 to 28, 2016. The model is constrained by hourly particle-phase data (without refractory ions and chloride) and gas-phase NH_3 and HNO_3 data, due to the low time-resolution of refractory ion and chloride concentrations (reported every 24 hours and not available every day). The average levels of refractory ions and chloride are low and similar to ANARChE. Therefore, they are not expected to have significant effects on pH. HCl concentration is also not available in SEARCH dataset. Description of SEARCH measurement techniques can be found in Table S1 in the supplement of Hidy et al. (2014).

2.3 SO_2, NO and NO_y Data

The ANARChE SO_2, NO and NO_y concentrations from August 1 to 31, 2002 were measured by commercial instruments (Thermo-Scientific). SO_2 concentrations were reported every 5 minutes and every 1 minute for NO and NO_y data. The detection limit of SO_2 was estimated to be 2 ppbv based on the observed variance in the observations. The SO_2 observations were over the maximum range of the instrument output from 12:00 pm to 12:55 pm on August 26 and were assigned to be 140 ppbv. Raw NO and NO_y data from the ANARChE archive were processed by subtracting background measurements and removing calibration points. Background signals were estimated by linear interpolation

between background measurements. The detection limits of NO and NO_y were estimated as 0.5 ppbv and 2 ppbv, respectively. All concentrations below the corresponding detection limit were replaced by half of the detection limit when calculating averages. The observations of NH_3, HNO_3, SO_2, NO and NO_y at the Jefferson Street site from August 1 to 31, 2016 were also utilized to investigate present day conditions to compare with the ANARChE results. The detection limits of NH_3, HNO_3, SO_2, NO and NO_y are 0.2-0.3 ppbv, 0.1 ppbv, 0.2 ppbv, 0.05 ppbv and 0.1 ppbv, respectively (Hansen et al., 2003; Saylor et al., 2010).

CHAPTER 3. RESULTS AND DISCUSSION

3.1 Decrease of SO_2, NO and NO_y Levels in the Past 15 Years

The time series of August SO_2, NO and NO_y concentrations from ANARChE and SEARCH dataset are shown in Figure 1 and Figure 2, respectively. Table 1 and Table 2 show the average concentrations (±SD), RH and T of ISORROPIA-II input from the ANARChE and SEARCH dataset. There is a large decrease in atmospheric concentrations of SO_2, NO and NO_y from 2002 to 2016, corresponding to the emissions reduction. The maximum SO_2, NO and NO_y in August 2002 were 140 (the instrument saturation level), 290 and 404 ppbv, while the maximum concentrations in August 2016 were 2, 89 and 129 ppbv. The average concentrations (±SD) were 6.6 ± 11.9 (SO_2), 13.8 ± 27.8 (NO) and 38.6 ± 39.0 ppbv (NO_y) in 2002 (medians of 2.5, 1.9, and 24.0 ppbv, respectively), higher than the averages of 0.2 ± 0.2 (SO_2), 2.5 ± 5.6 (NO) and 11.9 ± 10.6 ppbv (NO_y) (medians of 0.1, 0.5 and 8.1 ppbv) in 2016. Therefore, SO_2, NO and NO_y concentrations in August have decreased by approximately 97%, 82% and 69% from 2002 to 2016.

As shown in Table 2, the SEARCH sulfate and the sum of HNO_3 and NO_3^- concentrations are lower than ANARChE, especially for sulfate (decreased from 4.42 to 1.43 μg m^{-3}), which is consistent with the emissions reduction. Both NH_3 and NH_4^+ concentrations have also decreased by 21% and 65%, respectively. However, the SEARCH NH_3 measurement method is different from ANARChE and the measured concentrations are likely to be lower.

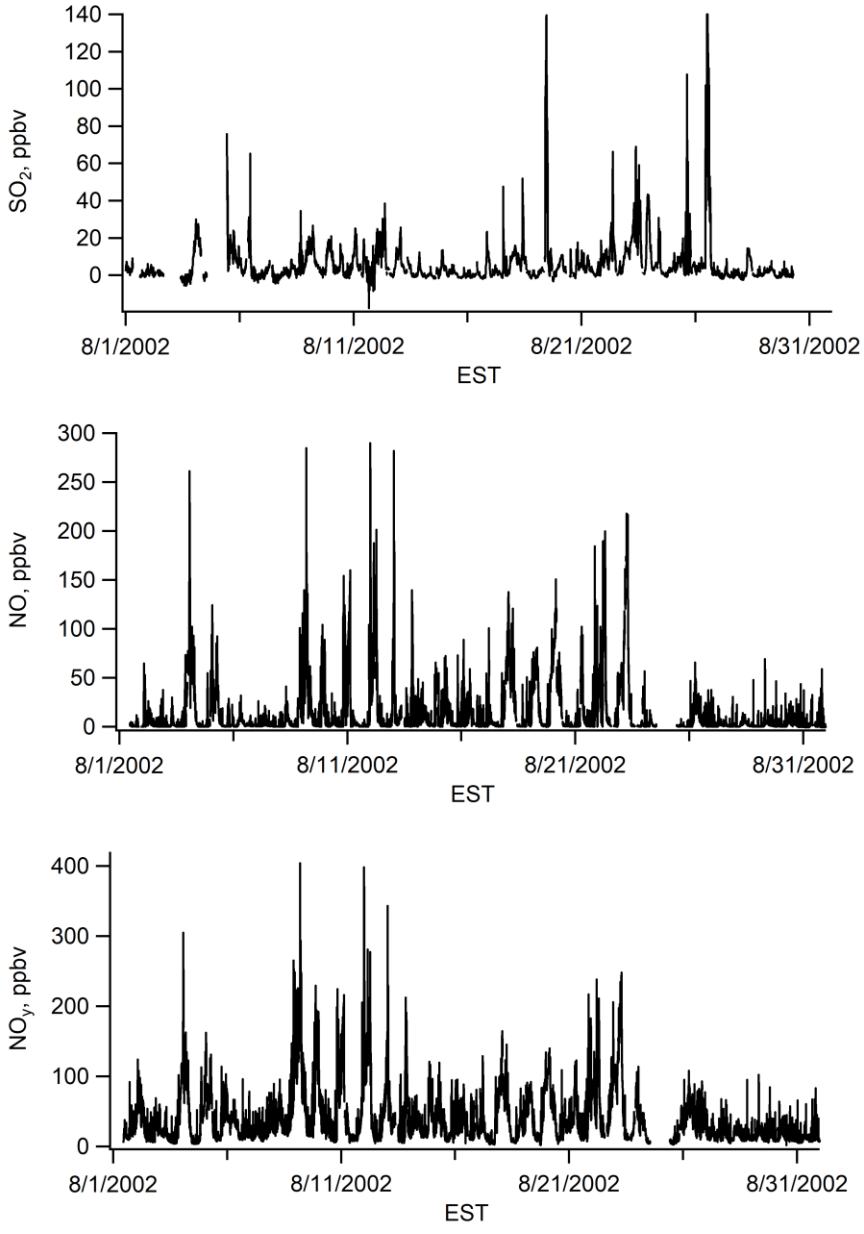

Figure 1 Time series of SO_2, NO and NO_y from ANARChE in August 2002.

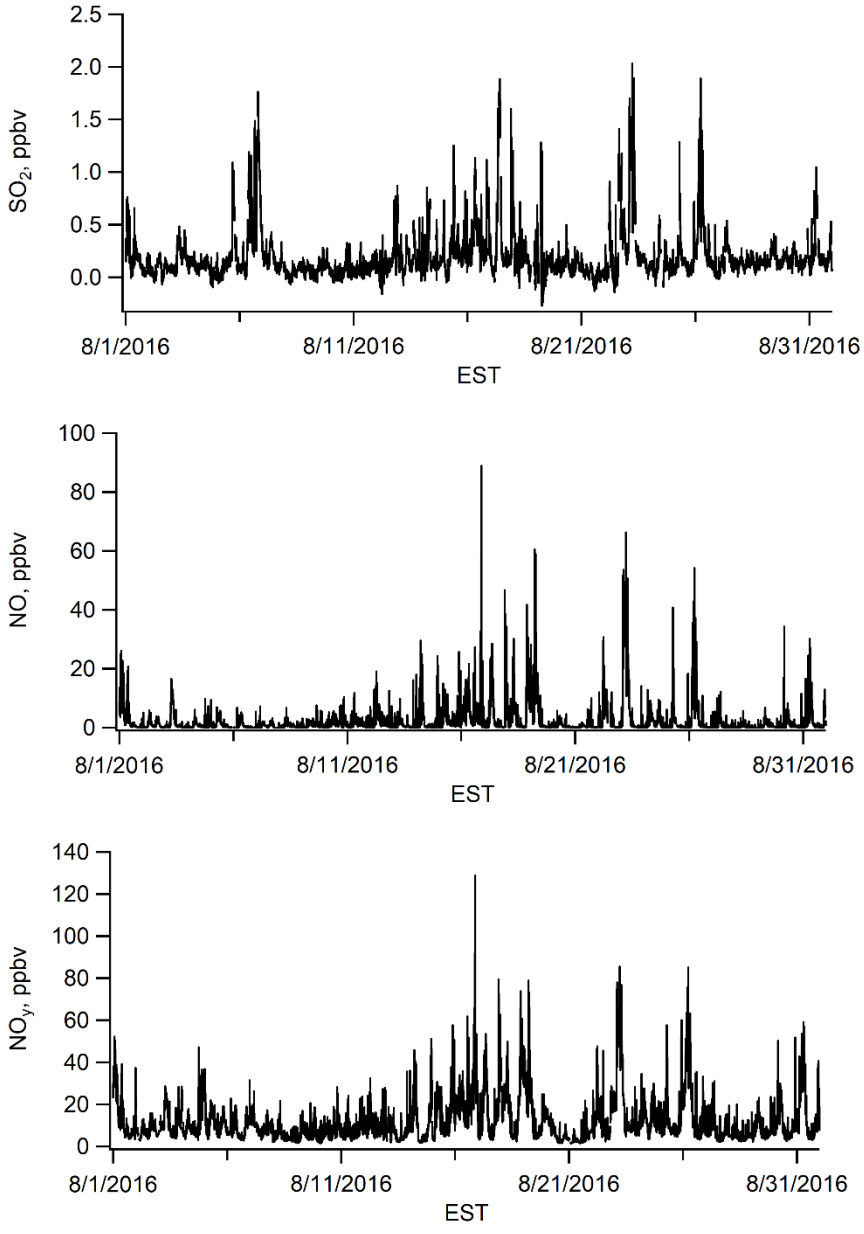

Figure 2 Time series of SO_2, NO and NO_y from SEARCH in August 2016.

Table 1 Average ANARChE concentrations (±SD), RH and T, from August 15 to 28, 2002.

Concentration, RH and T	Average (±SD)
RH, %	70 ± 16
Temperature, K	301.3 ± 4.0
Na^+, μg m^{-3}	0.06 ± 0.19
SO_4^{2-}, μg m^{-3}	4.42 ± 2.98
$NH_3 + NH_4^+$, μg m^{-3}	4.48 ± 1.53
NH_4^+, μg m^{-3}	2.13 ± 1.12
NH_3, μg m^{-3}	2.35 ± 0.96
$HNO_3 + NO_3^-$, μg m^{-3}	3.63 ± 2.09
NO_3^-, μg m^{-3}	0.35 ± 0.40
HNO_3, μg m^{-3}	3.28 ± 2.16
Cl^-, μg m^{-3}	0.05 ± 0.05
Ca^{2+}, μg m^{-3}	0.04 ± 0.04
K^+, μg m^{-3}	0.07 ± 0.06
Mg^{2+}, μg m^{-3}	0.02 ± 0.00

Table 2 Average SEARCH concentrations (±SD), RH and T, from August 15 to 28, 2016.

Concentration, RH and T	Average (±SD)
RH, %	71 ± 15
Temperature, K	300.5 ± 2.9
SO_4^{2-}, μg m^{-3}	1.43 ± 0.64
$NH_3 + NH_4^+$, μg m^{-3}	2.60 ± 0.77
NH_4^+, μg m^{-3}	0.75 ± 0.18
NH_3, μg m^{-3}	1.85 ± 0.73
$HNO_3 + NO_3^-$, μg m^{-3}	1.40 ± 0.75
NO_3^-, μg m^{-3}	0.23 ± 0.13
HNO_3, μg m^{-3}	1.17 ± 0.76

3.2 pH and Partitioning Fractions from the ANARChE Data

The average fine particle pH from August 15 to 28, 2002 is 1.92 ± 0.58 (±SD), with a median of 1.88. The partitioning fraction of semivolatile species, ε, is expressed as

$$\varepsilon(NH_4^+) = \frac{n(NH_4^+)}{n(NH_3) + n(NH_4^+)} \tag{3}$$

$$\varepsilon(NO_3^-) = \frac{n(NO_3^-)}{n(HNO_3) + n(NO_3^-)} \tag{4}$$

where n is the number of moles.

The diurnal cycles (average ± SD) of PM2.5 pH, W_i, RH, T, concentrations of NH_3, NH_4^+, HNO_3, NO_3^-, SO_2 and NO_y, and partitioning fractions of NH_4^+ and NO_3^- (August 15-28, 2002) are plotted in Figure 3, Figure 4 and Figure 5. Data used for the diurnal cycle calculation are the same as the input for pH calculation except for SO_2 and NO_y. Fine particle pH was higher at night and decreased after sunrise, with the highest (2.6) at 6 am and the lowest (1.2) at 2 pm. The pH correlated well with W_i, which is a nonlinear function of RH. Temperature and RH showed a negative correlation. Low RH and W_i occurred in the afternoon due to higher temperatures and thus H^+ becomes more concentrated in particle water, decreasing particle pH. The high RH and W_i in the early morning led to dilution and a higher pH. The hourly average of NH_3 started to increase in the morning and peaked at 3-5 pm, followed by a decrease at night. The NH_4^+ concentrations were a little higher during the day. Although pH exhibited a diurnal trend, there is no significant trend for $\varepsilon(NH_4^+)$ from observation. HNO_3 concentration peaked in the late afternoon and NO_3^- peaked in the morning, therefore $\varepsilon(NO_3^-)$ had a larger variation than $\varepsilon(NH_4^+)$ and its diurnal

trend was similar to pH, indicating that $\varepsilon(NO_3^-)$ has a higher sensitivity to pH. The hourly average of SO_2 concentration was the highest at midday, and had a smaller peak between 9-11 pm. The larger standard deviation at midday is due to intermittent SO_2 peaks. NO_y exhibited a peak during morning rush hour followed by a daytime decrease, and then a nighttime increase.

Figure 6 shows the ISORROPIA-II predicted vs. measured concentrations of NH_3, NH_4^+, HNO_3 and NO_3^-. The predicted vs. observed partitioning fractions of NH_4^+ and NO_3^- are also plotted. A linear regression using the singular value decomposition (SVD) algorithm is performed for each plot in Figure 6. The slope, intercept (± one standard deviation) and R^2 of the regression lines are labeled. Similar to Nowak et al. (2006), the agreement between predicted and measured NH_3 is good, with a slope of 1.29 and R^2 of 0.81. Generally, ISORROPIA-II underpredicted the ammonium concentrations and $\varepsilon(NH_4^+)$, with a slope of 0.73 and 0.72, respectively. Difference between the average $\varepsilon(NH_4^+)$ from measurement (44.6%) and model output (33.6%) is ~10.9%. The predicted HNO_3 concentrations have a very good agreement with measurements (slope = 1.00 and $R^2 = 0.97$), which is due to the high HNO_3 concentration compared to NO_3^-. Although the average differences between the observed and predicted NO_3^- and $\varepsilon(NO_3^-)$ are relatively small (slope = 0.83 for NO_3^- and 0.82 for $\varepsilon(NO_3^-)$), the NO_3^- and $\varepsilon(NO_3^-)$ data are scattered, with R^2 of 0.45 for NO_3^- and 0.46 for $\varepsilon(NO_3^-)$. This is probably due to the difficulty of measuring HNO_3.

The average observed $\varepsilon(NH_4^+)$ and $\varepsilon(NO_3^-)$ are 44.6 ± 16.8% and 13.5 ± 15.2%, respectively. Figure 6(c) and Figure 6(f) also demonstrate that most $\varepsilon(NO_3^-)$ values are low and $\varepsilon(NH_4^+)$ is distributed over a wide range of values. Therefore, when assessing model

validity, it is more useful to look at the phase partitioning of NH_3 instead of HNO_3 for the ANARChE data.

There are some data points (15 in total) on the left of Figure 6(c) with low observed $\varepsilon(NH_4^+)$ and a predicted $\varepsilon(NH_4^+)$ at around 50%. The prediction vs. observation graphs when these points are considered outliers are plotted in Figure 7. Only the regression of $\varepsilon(NH_4^+)$ showed a relatively large difference. A discussion about the outliers can be found in Appendix A. A series of sensitivity analysis was performed to evaluate potential sources of bias, where (1) the measured NH_3 concentrations were increased or decreased by 20%, (2) the HNO_3 concentrations were divided by two, (3) the refractory ions (Na^+, Ca^{2+}, K^+, Mg^{2+}) were excluded from model calculation, and (4) RH (0 to 1) was increased by 0.05 or 0.1. These cases were considered due to the NH_3 measurement uncertainty of 20%, measured HNO_3 higher than the actual, and the relatively lower predicted particle-phase NH_4^+ compared to observation. The RH of data in case 3 and 4 is below 90% instead of 95% to avoid supersaturation. Since LWC is not a linear function of RH, W_i could be orders of magnitude higher when the particle is supersaturated.

The average pH values in these cases are 2.0 ± 0.6 (120% NH_3), 1.8 ± 0.6 (80% NH_3), 1.9 ± 0.6 (50% HNO_3), 1.7 ± 0.5 (excluding refractory ions), 2.0 ± 0.5 (RH + 5%), and 2.1 ± 0.6 (RH + 10%). The predicted vs. measured concentrations and partitioning fractions from cases 1 and 2 are plotted in Figure A-1, Figure A-3 and Figure A-5. Figure A-7 to Figure A-12 show the sensitivities for cases 3 and 4. These cases did not show a significant improvement in the agreement between observation and model prediction, and most slopes and intercepts of the regression lines did not change much under the

perturbations except for NO_3^- and $\varepsilon(NO_3^-)$ in cases 2 and 4. Detailed description of sensitivities in each case is provided in Appendix A.

The interpolation of hourly HNO_3 data to PILS sampling frequency may introduce error as well. The NH_3 measurements could also be influenced by local sources such as people performing instrument maintenance. In addition, it can take 30 min for PM1 particles to reach equilibrium with the gas phase and even longer for larger particles (Fountoukis et al., 2009). To reduce these effects, data were averaged every hour. The model prediction vs. observation based on hourly averages are shown in Figure 8. The regressions did not change significantly except for $\varepsilon(NO_3^-)$ where the slope decreased from 0.82 to 0.62. NO_3^- and $\varepsilon(NO_3^-)$ data points are still scattered, and the overprediction of NH_3 remained. Therefore, averaging to longer time periods was not found to improve conditions.

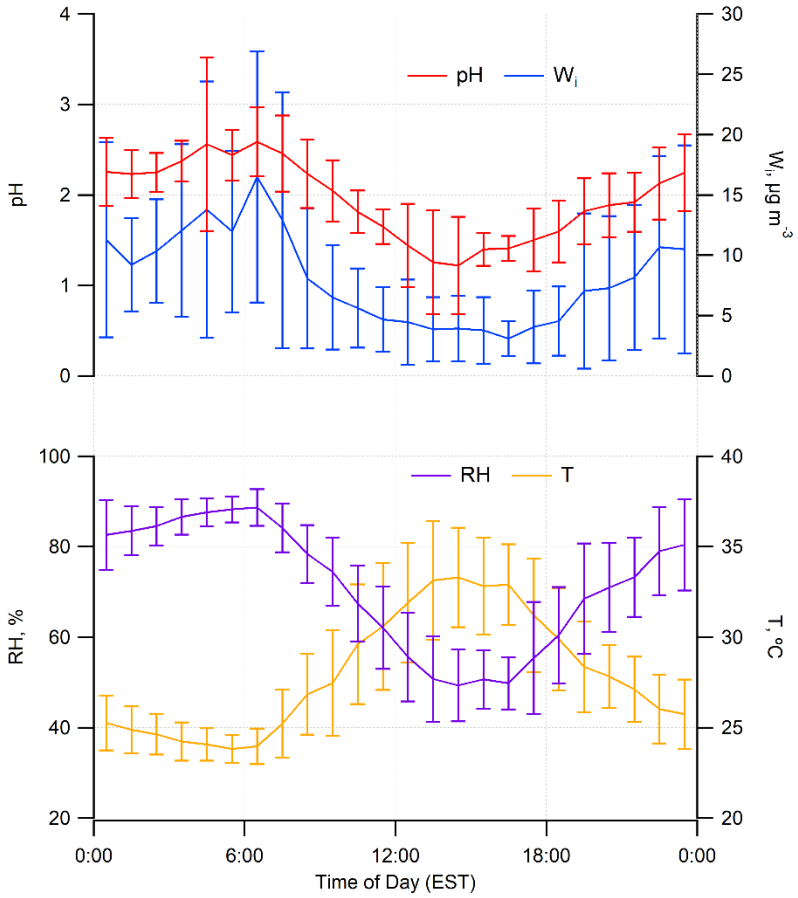

Figure 3 Diurnal cycles of fine particle pH, W_i, RH and T (average ± SD), from August 15 to 28, 2002.

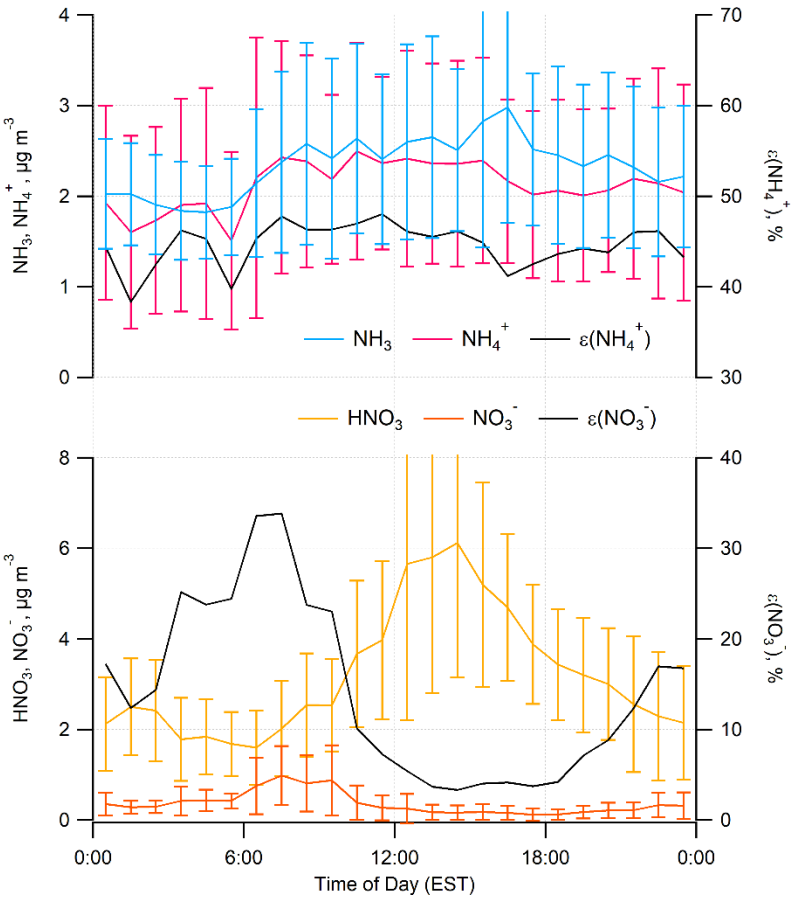

Figure 4 Diurnal cycles of fine particle NH_3, NH_4^+, HNO_3 and NO_3^- concentrations, as well as observed partitioning fractions $\varepsilon(NH_4^+)$ and $\varepsilon(NO_3^-)$ (average ± SD), from August 15 to 28, 2002.

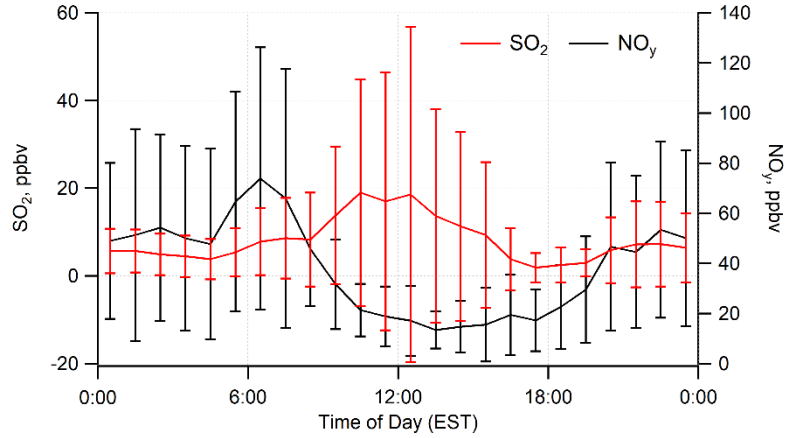

Figure 5 Diurnal cycles of SO_2 and NO_y (average ± SD), from August 15 to 28, 2002.

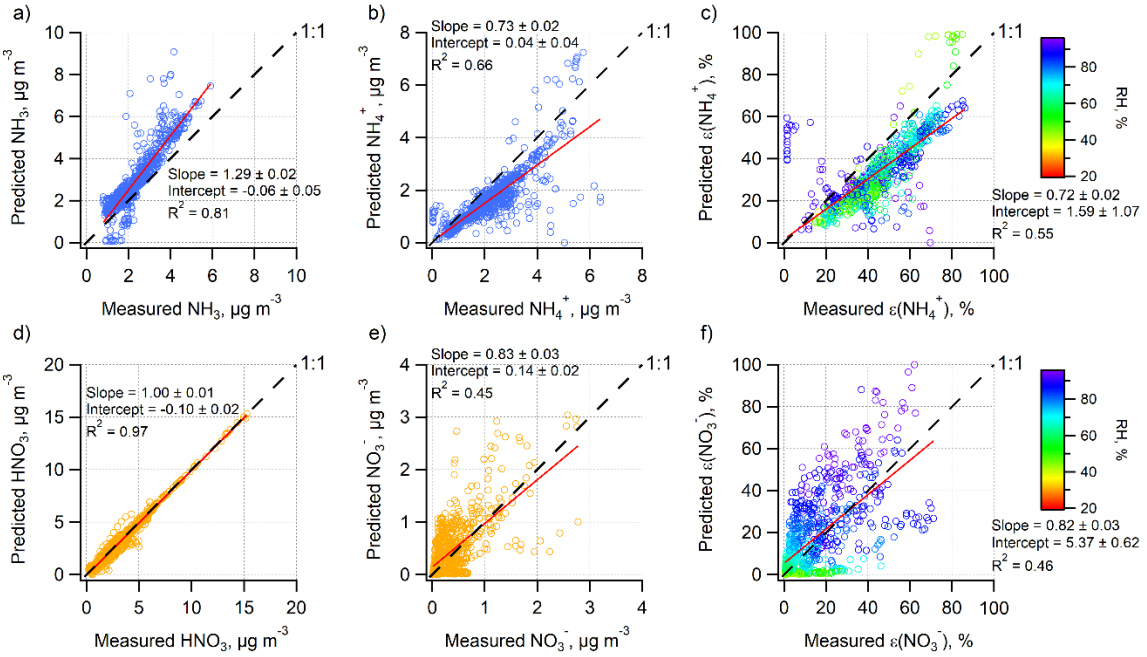

Figure 6 Predicted vs. observed ANARChE concentrations of NH_3 (a), NH_4^+ (b), HNO_3 (d) and NO_3^- (e), as well as partitioning fractions $\varepsilon(NH_4^+)$ (c) and $\varepsilon(NO_3^-)$ (f). Red line: linear regression based on SVD algorithm. Black dashed line: 1:1 line.

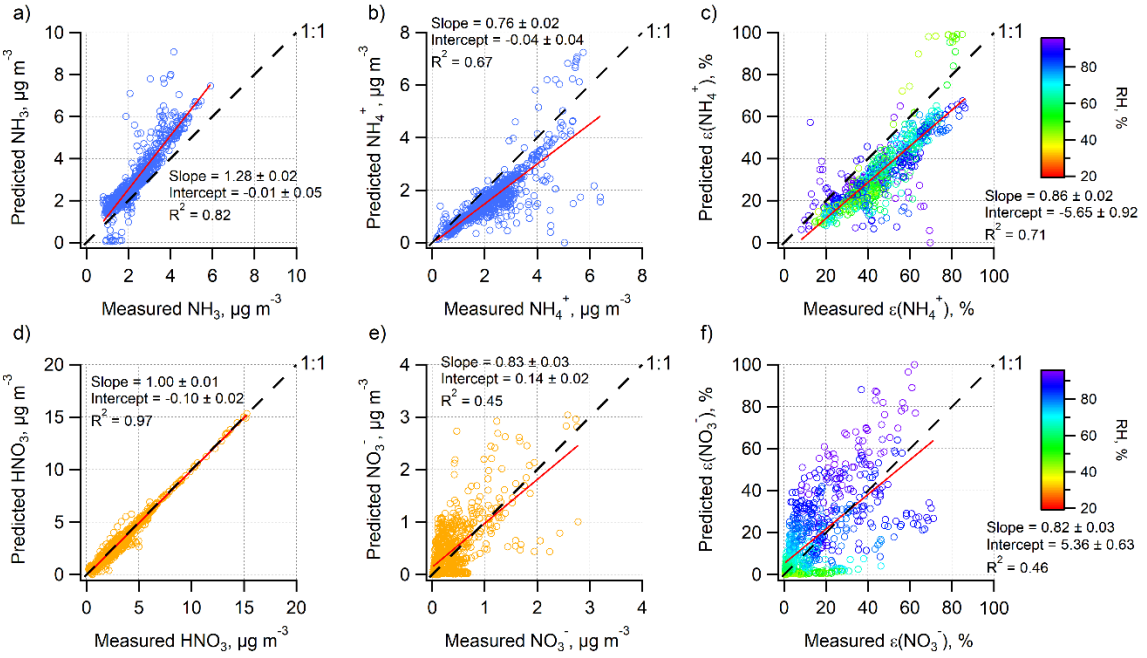

Figure 7 Same as Figure 6 (original data with RH < 95%). The low observed $\varepsilon(NH_4^+)$ outliers are removed from each graph.

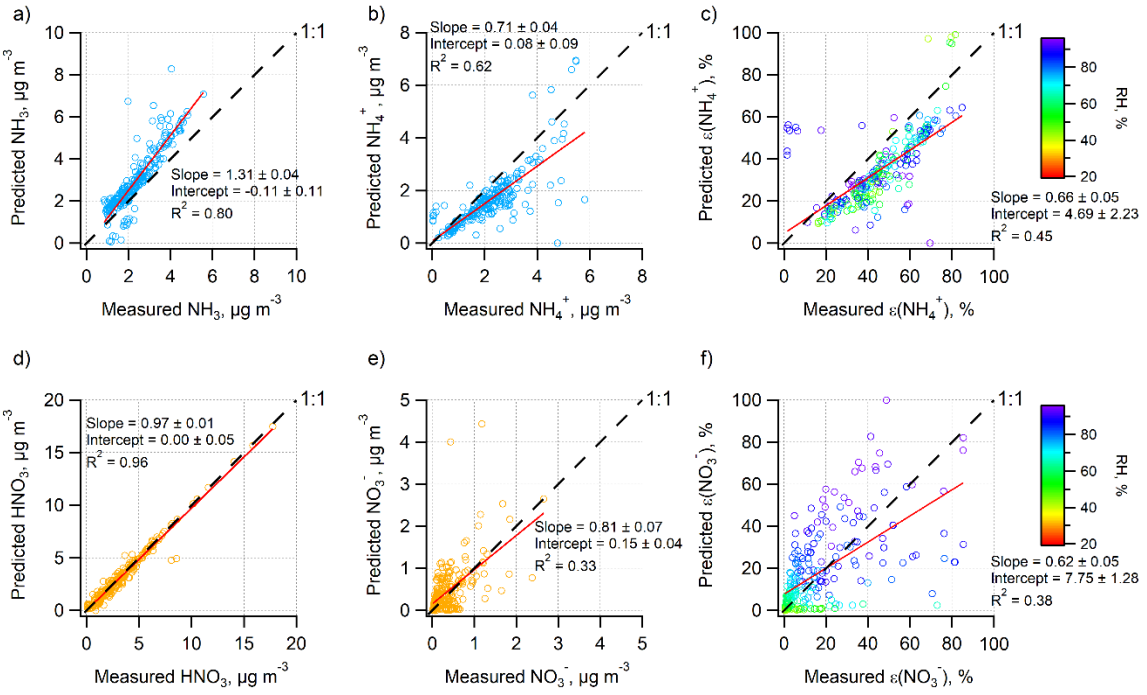

Figure 8 Same as Figure 6, but for hourly averaged data.

3.3 pH and Partitioning Fractions from the SEARCH Data

The average pH for SEARCH dataset is 1.68 ± 0.48, with a median of 1.67. It should be noted that it is likely the pH would only slightly increase if refractory ions and chloride were included (a discussion is provided in 3.4). The pH averages (±SD) and medians from the ANARChE and SEARCH data are plotted in Figure 9. This result is only slightly lower than ANARChE, especially considering the accuracy of the method. Therefore, the summertime fine particle pH in urban Atlanta only seemed to decrease a small amount despite the large cuts in acid precursors (NO_x and SO_2). It is also worth noting that the average NH_4^+ partitioning fraction from SEARCH observation is 29.5% that is

lower than ANARChE (44.6%). This suggests the volatilization of NH_4^+ increases with lower particle mass loadings, which compensates for the effect of SO_4^{2-} decrease on pH.

The diurnal cycles (Figure 10 and Figure 11) of the SEARCH data are similar to the ANARChE results except for the lower W_i and the larger $\varepsilon(NH_4^+)$ diurnal variation. The average predicted W_i for the SEARCH data is 2.3 μg m^{-3} that is lower than the average of 7.9 μg m^{-3} from ANARChE, which is mainly due to the sulfate level decrease. The $\varepsilon(NH_4^+)$ peak in the afternoon is consistent with a lower pH. Although the $\varepsilon(NH_4^+)$ diurnal variation is larger compared with ANARChE, it is still less sensitive to the change in pH than $\varepsilon(NO_3^-)$.

The relationship between predicted and observed values from SEARCH dataset is shown in Figure 12. NH_3 is also slightly overestimated but data points are closer to the 1:1 line, and the slope (0.95) is closer to 1. The R^2 became higher (0.98 compared to 0.81). The model underestimated NH_4^+ concentration and $\varepsilon(NH_4^+)$. As shown in Figure 12, the $\varepsilon(NH_4^+)$ points are concentrated in the < 50% region, while the $\varepsilon(NH_4^+)$ from ANARChE has a wider range and the average is higher. Similar to ANARChE, the agreement between predicted and measured HNO_3 is good (slope of 1.01, intercept of 0.17 and R^2 of 0.98). However, the predicted NO_3^- and $\varepsilon(NO_3^-)$ are much lower than observation (slope of 0.28 and 0.36, respectively, lower than the slopes from hourly averaged ANARChE data). The average predicted $\varepsilon(NO_3^-)$ is 5.1% that is lower than the observed average of 21.3%.

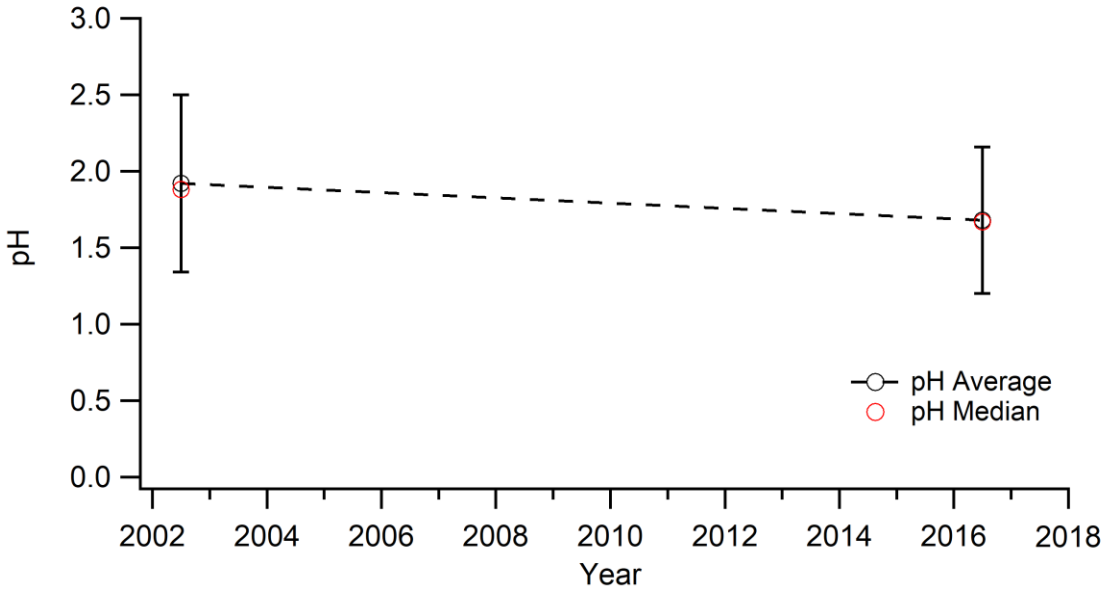

Figure 9 The pH averages (±SD) and medians of the ANARChE and SEARCH data.

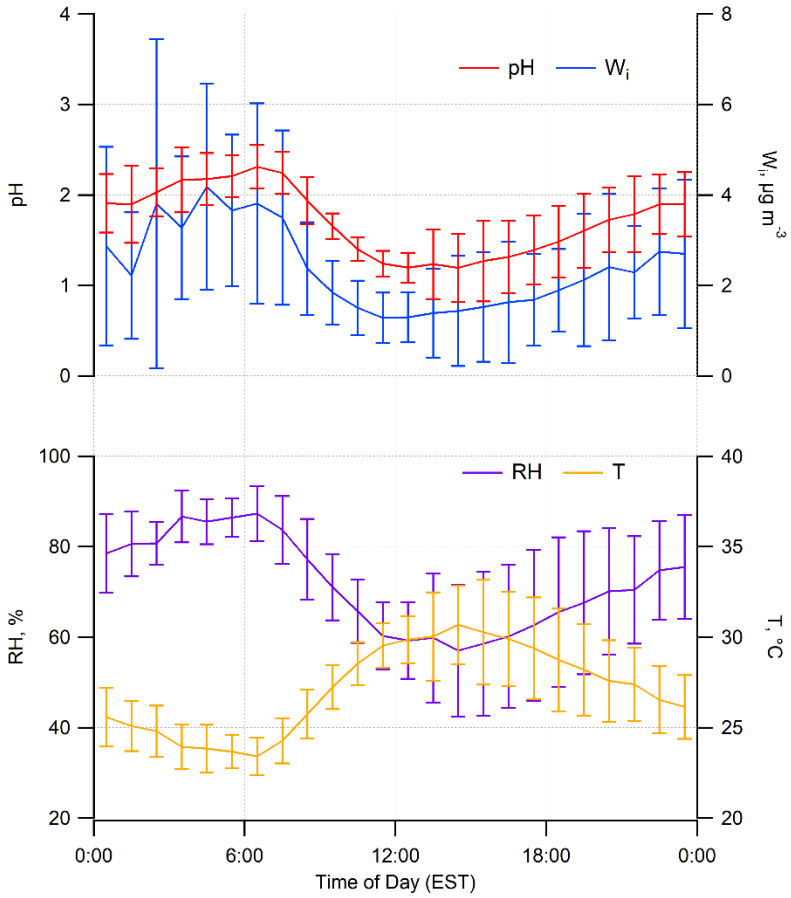

Figure 10 Diurnal cycles of fine particle pH, W_i, RH and T (average ± SD), from August 15 to 28, 2016.

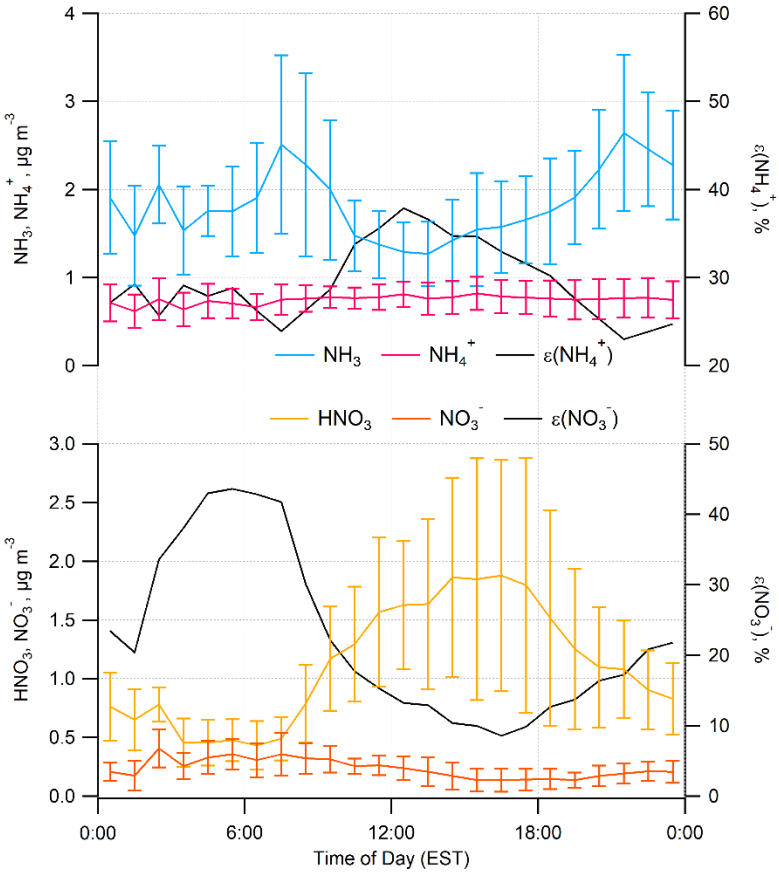

Figure 11 Diurnal cycles of fine particle NH_3, NH_4^+, HNO_3 and NO_3^- concentrations, as well as observed partitioning fractions $\varepsilon(NH_4^+)$ and $\varepsilon(NO_3^-)$ (average ± SD), from August 15 to 28, 2016.

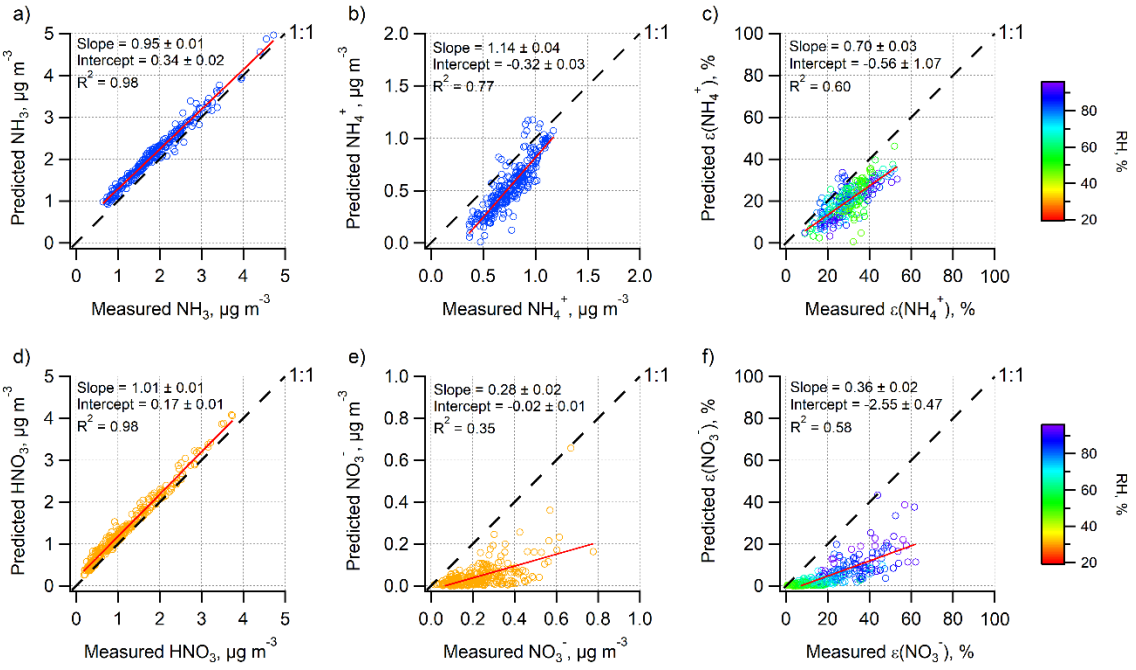

Figure 12 Prediction vs. observation from hourly SEARCH data.

3.4 Effects of Concentrations on Particle pH

To evaluate the effects of refractory ions and gas-phase data on calculated particle pH, data excluding refractory ions (i.e. gas + particle phase NH_3, HNO_3, Cl^-, and SO_4^{2-} as input), and data without both gas-phase concentrations and refractory ions (i.e. only particle phase NH_4^+, NO_3^-, Cl^-, and SO_4^{2-} as input) were also calculated. Excluding refractory ions only decreased pH by ~0.1 units (pH average of 1.81 ± 0.55, median of 1.77), while particle pH decreased to 1.01 ± 0.63 (median of 1.02) if neither gas-phase data nor refractory ions were considered. This result is comparable with the pH decrease by 0.0 to 0.4 units without crustal ions (K^+, Ca^{2+}, Mg^{2+}) from Liu et al. (2017), and also similar to the pH increase of

0.8 units when the model is further constrained by gas-phase NH_3 in addition to particle-phase data (Guo et al., 2015).

Based on the average PM2.5 pH of this study, it cannot be concluded that fine particle has been less acidic in recent years due to the SO_2 and NO_x emission reduction. During SOAS in 2013, fine particle pH at Centreville (CTR), Alabama is predicted to be 0.94 ± 0.59 (Guo et al., 2015), and the time evolution of particle pH at the same site from 1998 to 2013 has a range of 0 – 2 pH units (Weber et al., 2016). Aerosol compositions at several sites in Atlanta including Jefferson Street were also measured as part of the Southeastern Center for Air Pollution and Epidemiology (SCAPE) study in 2012. The average predicted pH at JST site in May 2012 was reported as 1.3 ± 0.7, and for another site on the rooftop of the Ford Environmental Science and Technology building (Georgia Institute of Technology, GIT site) 2 km east of JST site, the predicted pH was 1.1 ± 0.4 in August 2012 (Guo et al., 2015).

Due to the small effect of refractory ions on pH, the higher fine particle pH during ANARChE than the other studies may be explained by the difference in gas + particle phase NH_3, HNO_3 and SO_4^{2-}. Figure 3 in Weber et al. (2016) shows that at fixed RH, T, and concentrations of Na^+, NO_3^- and Cl^- (at SOAS mean), pH increases with NH_3(g) and decreases with increasing SO_4^{2-}. The average total NH_3 (NH_3 + NH_4^+), HNO_3 (HNO_3 + NO_3^-) and SO_4^{2-} for ANARChE pH calculation are 4.48 μg m^{-3}, 3.63 μg m^{-3}, and 4.42 μg m^{-3}, respectively, which are higher than the average of SOAS (a rural site with total NH_3 of 0.78 μg m^{-3}, total HNO_3 of 0.45 μg m^{-3}, and SO_4^{2-} of 1.73 μg m^{-3}) (Guo et al., 2017a). A sensitivity test was performed to estimate the effects of total NH_3, HNO_3 and SO_4^{2-}. By inputting the averages listed in Table 1, the model predicted a pH of 1.83, while after

changing total HNO_3, total NH_3 and SO_4^{2-} separately into SOAS average concentration, the predicted pH became 1.79, 0.08 and 2.08. Excluding refractory ions resulted in a pH of 1.75. Therefore, higher total HNO_3 did not have a significant effect on raising particle pH under ANARChE conditions, and pH is mainly controlled by total NH_3 and SO_4^{2-}.

To explain the similar pH between ANARChE and SEARCH data, the sensitivities of particle pH to concentration variations are tested using the average concentrations, RH and T of the two datasets. The ANARChE and SEARCH datasets have similar average RH and T. The pH based on SEARCH averages in Table 2 is 1.62, almost the same as the average pH of 1.68. Including refractory ion and chloride concentrations (annual average in 2016 based on 24h data, Na^+: 0.05 μg m^{-3}, Cl^-: 0.04 μg m^{-3}, Ca^{2+}: 0.03 μg m^{-3}, K^+: 0.03 μg m^{-3}, Mg^{2+}: 0.01 μg m^{-3}) increased pH to 1.74, and pH increased to 1.84 when average refractory ion and chloride concentrations from ANARChE were included.

The pH increased to 1.92 by only increasing total NH_3 to the average ANARChE level, and W_i slightly increased from 1.79 to 1.81 μg m^{-3}. Therefore, pH is not sensitive to the increase in total NH_3 under ANARChE/SEARCH conditions. The ANARChE averages excluding refractory ions and chloride resulted in a pH of 1.75. By only decreasing sulfate and total HNO_3 to SEARCH level, pH increased to 1.87 and W_i decreased from 5.49 to 1.74 μg m^{-3}. The decrease of W_i is mainly due to sulfate, which may also account for the small pH increase since the lower liquid water content would lead to more concentrated H^+. This is supported by the average W_i of 2.3 μg m^{-3} from SEARCH data, much lower than W_i of 7.9 μg m^{-3} from ANARChE. Similar to the decrease in the observed $\varepsilon(NH_4^+)$, the predicted NH_4^+ partitioning fraction decreased from 35.8% to 11.3% in the sensitivity test, despite the same total NH_3 concentration.

3.5 S Curve, Partitioning Fractions Dependence on pH

A detailed derivation of theoretical $\varepsilon(NO_3^-)$ and $\varepsilon(NH_4^+)$ sigmoid calculations is provided in the supplement of Guo et al. (2017a). Briefly, the $\varepsilon(NO_3^-)$ and $\varepsilon(NH_4^+)$ equations used in this study are

$$\varepsilon(NO_3^-) \cong \frac{H^*_{\mathrm{HNO_3}} W_\mathrm{i} RT \times 0.987 \times 10^{-14}}{\gamma_{\mathrm{NO_3^-}}\gamma_{\mathrm{H^+}} 10^{-\mathrm{pH}} + H^*_{\mathrm{HNO_3}} W_\mathrm{i} RT \times 0.987 \times 10^{-14}} \tag{5}$$

$$\varepsilon(NH_4^+) \cong \frac{\frac{\gamma_{\mathrm{H^+}} 10^{-\mathrm{pH}}}{\gamma_{\mathrm{NH_4^+}}} H^*_{\mathrm{NH_3}} W_\mathrm{i} RT \times 0.987 \times 10^{-14}}{1 + \frac{\gamma_{\mathrm{H^+}} 10^{-\mathrm{pH}}}{\gamma_{\mathrm{NH_4^+}}} H^*_{\mathrm{NH_3}} W_\mathrm{i} RT \times 0.987 \times 10^{-14}} \tag{6}$$

where $\gamma_{\mathrm{H^+}}$, $\gamma_{\mathrm{NO_3^-}}$, and $\gamma_{\mathrm{NH_4^+}}$ are activity coefficients of H^+, NO_3^-, and NH_4^+, respectively, R the universal gas constant, W_i the inorganic liquid water content in μg m^{-3} air, T the temperature in Kelvin. $H^*_{\mathrm{HNO_3}}$ in $mol^2\ kg^{-2}\ atm^{-1}$ and $H^*_{\mathrm{NH_3}}$ in atm^{-1} can be calculated from Clegg and Brimblecombe (1990) and Clegg et al. (1998). The 0.987×10^{-14} term is the combination of conversion factors from atm to Pa and from μg to kg. ISORROPIA-II exported the mean activity coefficients $\gamma_{\mathrm{HNO_3}}$ and $\gamma_{\mathrm{NH_4NO_3}}$. Their averages and standard deviations are used for sigmoid calculations:

$$\gamma_{\mathrm{NO_3^-}}\gamma_{\mathrm{H^+}} = \gamma^2_{\mathrm{HNO_3}} \tag{7}$$

$$\frac{\gamma_{\mathrm{H^+}}}{\gamma_{\mathrm{NH_4^+}}} = \frac{\gamma_{\mathrm{H^+}}\gamma_{\mathrm{NO_3^-}}}{\gamma_{\mathrm{NH_4^+}}\gamma_{\mathrm{NO_3^-}}} = \frac{\gamma^2_{\mathrm{HNO_3}}}{\gamma^2_{\mathrm{NH_4NO_3}}} \tag{8}$$

The theoretical $\varepsilon(NH_4^+)$ and $\varepsilon(NO_3^-)$ using average T and W_i of the whole ANARChE dataset, along with practical activity coefficients from ISORROPIA-II are plotted as blue solid lines in Figure 13(a) and Figure 14(a). The blue dashed lines indicate sigmoid curves calculated from $\gamma_{HNO_3} + \sigma_{\gamma_{HNO_3}}$ and $\gamma_{NH_4NO_3} + \sigma_{\gamma_{NH_4NO_3}}$, or from $\gamma_{HNO_3} - \sigma_{\gamma_{HNO_3}}$ and $\gamma_{NH_4NO_3} - \sigma_{\gamma_{NH_4NO_3}}$. The red solid line is the ideal solution case, where all activity coefficients equal one. To illustrate the pH effect on partitioning fractions, the observed $\varepsilon(NH_4^+)$ and $\varepsilon(NO_3^-)$ of a small subset within average T ± 2 K (299.3 – 303.3 K) and average W_i ± 5 μg m^{-3} (2.9 – 12.9 μg m^{-3}) are plotted in Figure 13(a) and Figure 14(a) as well. The $\varepsilon(NH_4^+)$ points are close to the sigmoid curve while larger discrepancy occurs at higher RH. The observed $\varepsilon(NO_3^-)$ values are generally lower than the sigmoid curve.

The uncertainty of the NH_3 measurement is within 20%, and the measured HNO_3 concentration is thought to be much higher than the actual. To evaluate the effect of NH_3 and HNO_3 measurement uncertainties, three cases were considered (same as cases 1 and 2 in Appendix A): (1) the HNO_3 concentrations were divided by two (Figure 13(b) and Figure 14(b)), (2) 80% of measured NH_3 concentrations (Figure 13(c) and Figure 14(c)), (3) 120% of measured NH_3 concentrations (Figure 13(d) and Figure 14(d)). The S curves were calculated for each case based on the average T, W_i, and activity coefficients after the change. The observed $\varepsilon(NH_4^+)$ and $\varepsilon(NO_3^-)$ from the same subset as previous were plotted in order to show the shift of data points.

As shown in Figure 13 and Figure 14, varying NH_3 and HNO_3 concentrations did not have a significant effect on theoretical $\varepsilon(NH_4^+)$ and $\varepsilon(NO_3^-)$ curves, due to little change in average W_i and γ (average W_i, γ_{HNO3}, and γ_{NH4NO3} of 7.9 μg m^{-3}, 0.31 ± 0.06, and 0.26

± 0.04 without perturbation). The average W_i values for half HNO_3, 80% NH_3 and 120% NH_3 cases are 7.4, 7.7, and 8.0 μg m^{-3}, respectively. The average γ_{HNO3} values are 0.30 ± 0.06, 0.31 ± 0.08, and 0.31 ± 0.06. For all three cases, the average γ_{NH4NO3} values are 0.26 ± 0.04.

By definition, the observed $\varepsilon(NH_4^+)$ would not change when varying HNO_3 concentrations, and $\varepsilon(NO_3^-)$ would not change with NH_3 variation. When decreasing NH_3 concentration by 20%, data points shifted toward lower pH and higher $\varepsilon(NH_4^+)$. When increasing NH_3 concentration by 20%, data points shifted toward the opposite direction. The agreement between observed and theoretical $\varepsilon(NO_3^-)$ became better when using half HNO_3 concentration since the observed $\varepsilon(NO_3^-)$ increased.

To evaluate the pH effect on particle-phase NH_4^+ and NO_3^- levels, the predicted $\varepsilon(NH_4^+)$ and $\varepsilon(NO_3^-)$ vs. pH from the original whole dataset are plotted in Figure 15. A sigmoid curve fitting was performed using the equations below, which is based on the theoretical sigmoid equations.

$$\varepsilon(NH_4^+) = \frac{a \times 10^{-pH}}{1 + a \times 10^{-pH}} \times 100\% \quad (9)$$

$$\varepsilon(NO_3^-) = \frac{a}{b \times 10^{-pH} + a} \times 100\% \quad (10)$$

The initial guess (magnitude only) of fit coefficients *a* and *b* using average T, W_i and activity coefficients are 42.0214 for $\varepsilon(NH_4^+)$, 3.7771×10^{-4} (*a*) and 0.0958 (*b*) for $\varepsilon(NO_3^-)$. Final fit coefficients values are 23.273 for $\varepsilon(NH_4^+)$, 2.23×10^{-4} (*a*) and 0.137 (*b*) for $\varepsilon(NO_3^-)$.

The change in particle-phase concentrations with pH variation can be calculated from the partitioning fractions based on regression equations and gas + particle phase concentrations. The average observed NH_3 + NH_4^+ and HNO_3 + NO_3^- are 4.48 and 3.63 μg m^{-3}, respectively. Particle-phase concentration variations when pH increases or decreases by one unit (i.e. 2.92 and 0.92) are listed in Table 3.

Table 3 Particle-phase concentration variations with pH based on regression equations.

pH	ε(NH_4^+), %	ε(NO_3^-), %	NH_4^+, μg m^{-3}	NO_3^-, μg m^{-3}
0.92	73.7	1.3	3.30	0.05
1.92	21.9	12.0	0.98	0.43
2.92	2.7	57.6	0.12	2.09

The average NH_4^+ concentration (0.98 μg m^{-3}) from regression equation is lower than the average concentration from measurement (2.13 μg m^{-3}) due to model underprediction of NH_4^+ and the scattered data. The average NO_3^- concentrations are similar (0.43 μg m^{-3} from regression equation and 0.35 μg m^{-3} from measurement). NO_3^- concentration is sensitive to pH increase, and more nitrate formation is expected when pH approaches 3.

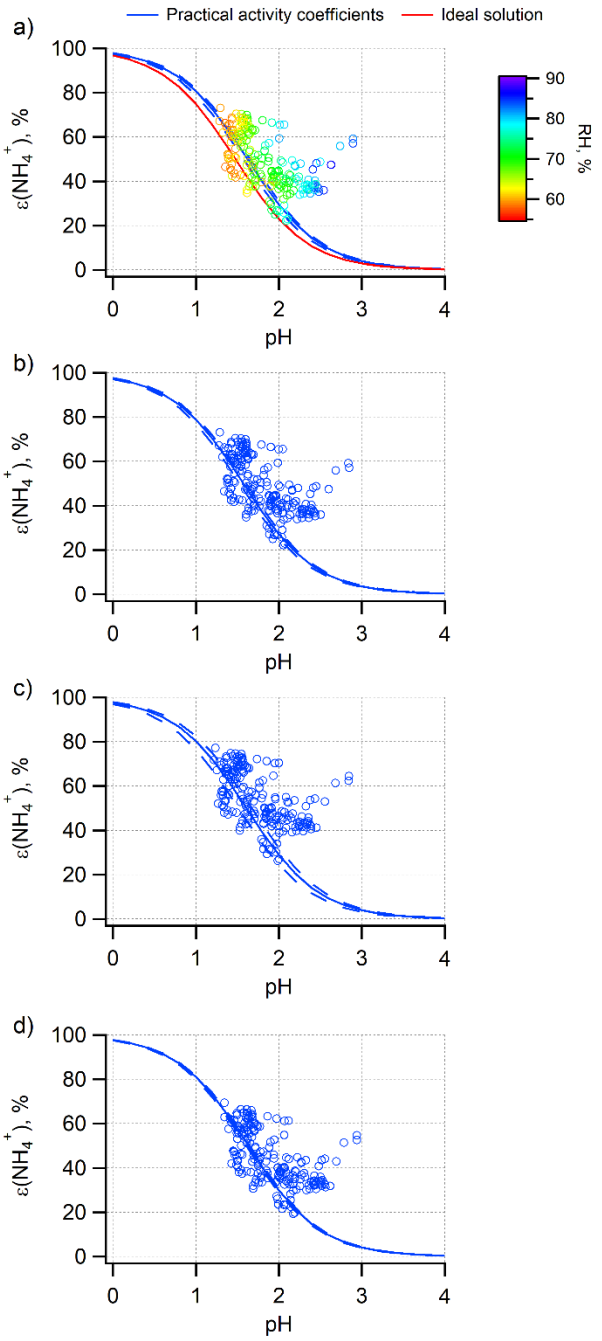

Figure 13 The partitioning fraction of NH_4^+ ($\varepsilon(NH_4^+)$) as a function of pH (blue solid line) based on average T, ISORROPIA-II predicted W_i and γ of the whole ANARChE dataset (a) without perturbation, (b) with 50% HNO_3, (c) 80% NH_3 and (d) 120% NH_3. S curves based on average T, W_i, γ_{HNO3} + σ and γ_{NH4NO3} + σ, or γ_{HNO3} − σ and γ_{NH4NO3} − σ for each case are indicated by blue dashed line. Red line: ideal solution case. Open circles: measured $\varepsilon(NH_4^+)$ from a subset (T from 299.3 to 303.3 K and W_i from 2.9 to 12.9 μg m^{-3}, same subset for all cases).

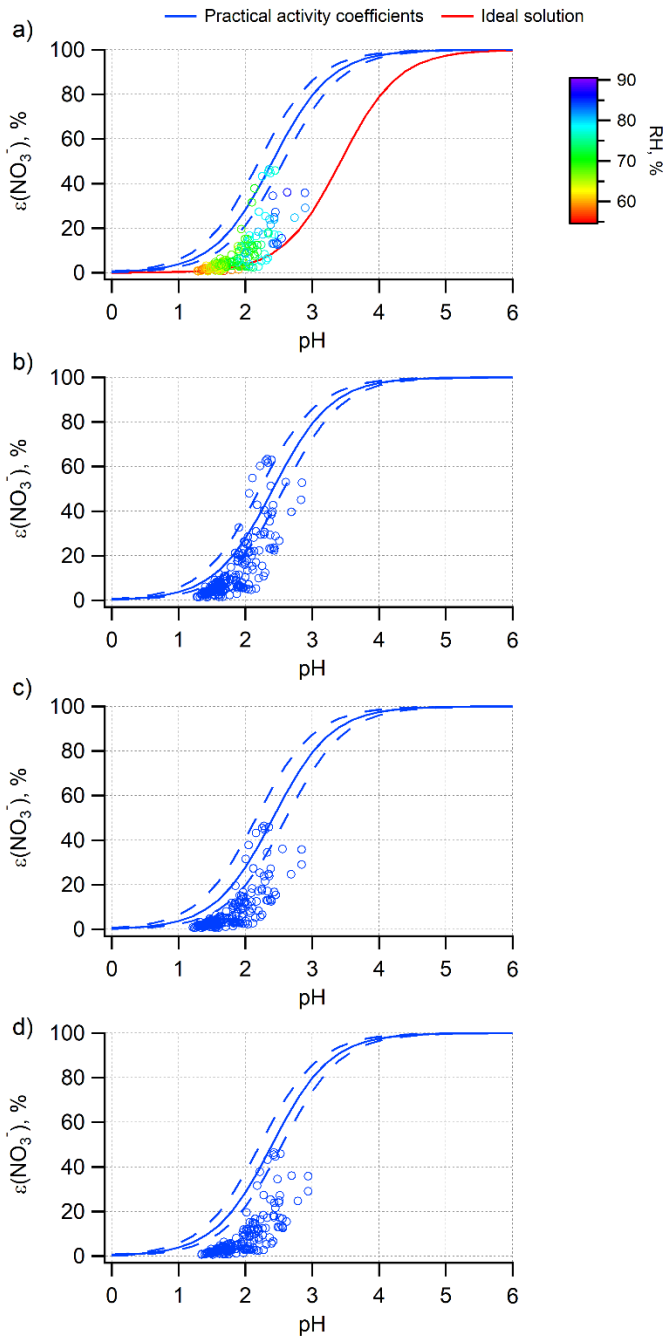

Figure 14 The partitioning fraction of NO_3^- ($\varepsilon(NO_3^-)$) as a function of pH (blue solid line) based on average T, ISORROPIA-II predicted W_i and γ of the whole ANARChE dataset (a) without perturbation, (b) with 50% HNO_3, (c) 80% NH_3 and (d) 120% NH_3. S curves based on average T, W_i, γ_{HNO3} + σ and γ_{NH4NO3} + σ, or γ_{HNO3} − σ and γ_{NH4NO3} − σ for each case are indicated by blue dashed line. Red line: ideal solution case. Open circles: measured $\varepsilon(NO_3^-)$ from a subset (T from 299.3 to 303.3 K and W_i from 2.9 to 12.9 μg m^{-3}, same subset for all cases).

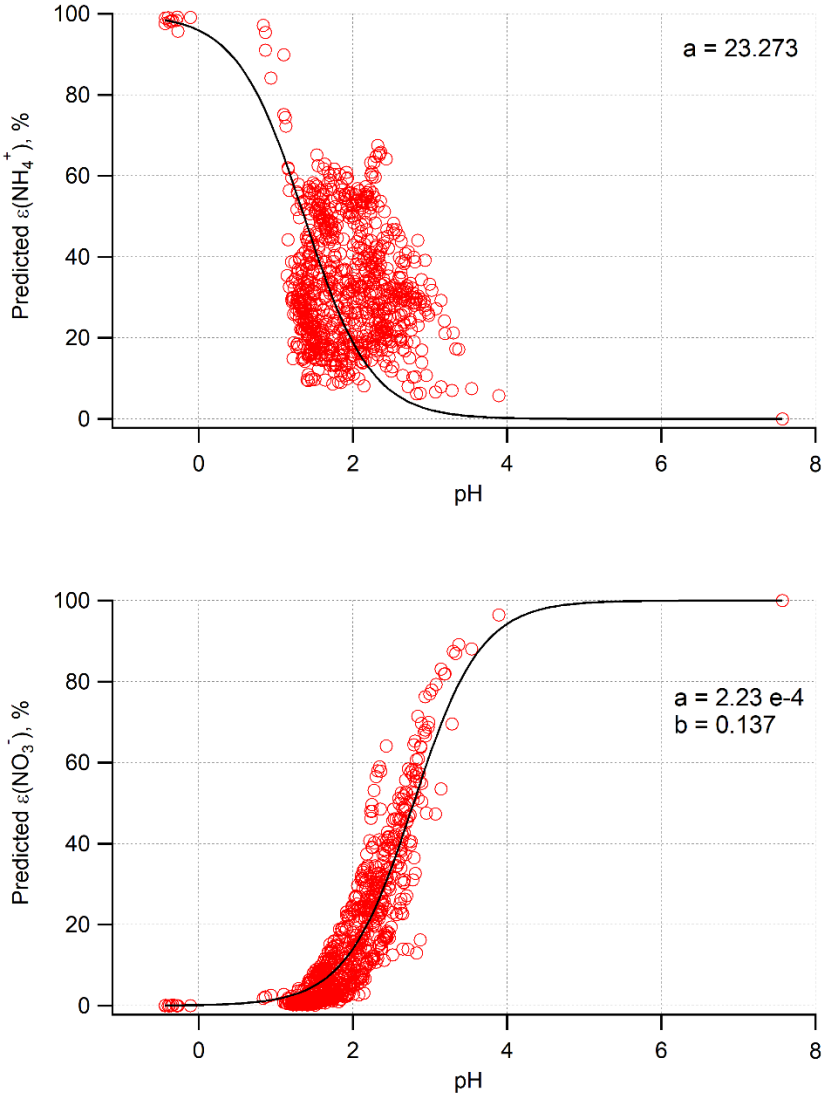

Figure 15 The predicted ANARChE $\varepsilon(NH_4^+)$ and $\varepsilon(NO_3^-)$ as a function of pH. The whole dataset from August 15 to 28 is plotted. S curve fitting based on equations (9) and (10) was performed and plotted as black line.

CHAPTER 4. CONCLUSIONS

In this study, the ANARChE data in August 2002 and SEARCH data in August 2016 collected at the Jefferson Street site, Atlanta were analyzed to investigate the change in pH over the past 15 years. Comparing the measured SO_2, NO and NO_y in August 2002 and 2016, the average concentrations have decreased from 6.6, 13.8 and 38.6 ppbv to 0.2, 2.5 and 11.9 ppbv, respectively (97% decrease for SO_2, 82% for NO and 69% for NO_y). The particle-phase sulfate has decreased from 4.42 to 1.43 μg m^{-3}, consistent with the change in SO_2 concentrations. The NH_3 + NH_4^+ concentrations have decreased from 4.48 to 2.60 μg m^{-3}.

The summertime fine particle pH based on ANARChE data (August 15-28, 2002) and SEARCH data (August 15-28, 2016) is calculated by ISORROPIA-II, a thermodynamic equilibrium model. The model was run in forward and metastable mode for data with RH < 95%. For ANARChE, the model was constrained by particle-phase concentrations including SO_4^{2-}, NH_4^+, NO_3^-, Cl^- and refractory ions, as well as gas-phase NH_3 and HNO_3 data. The chloride and refractory ion concentrations are not available in SEARCH dataset. The average fine particle pH from ANARChE is 1.92 ± 0.58 (±SD), with a median of 1.88. The average pH from SEARCH is 1.68 ± 0.48, with a median of 1.67. The SEARCH pH could be a little higher if refractory ions were considered. The results did not show a large change in fine particle pH, and the pH has slightly decreased despite the emission reduction of SO_2 and NO_x over the past 15 years. Comparing the average concentrations from the two datasets, the average fine particle sulfate, ammonium and nitrate levels have decreased from 4.42 to 1.43 μg m^{-3}, 2.13 to 0.75 μg m^{-3}, and 0.35 to

0.23 μg m^{-3}, respectively. The NH_3 and HNO_3 concentrations have decreased from 2.35 to 1.85 μg m^{-3}, and 3.28 to 1.17 μg m^{-3}. There is a large decrease in W_i (from 7.9 to 2.3 μg m^{-3}) that is mainly caused by the decrease in sulfate. The average observed $\varepsilon(NH_4^+)$ decreased from 44.6% to 29.5%, suggesting the volatilization of NH_4^+ which could compensate for part of the effects of decreasing SO_4^{2-}. The small change in particle pH could then be explained by the above-mentioned decrease in W_i and NH_4^+ volatilization. The observed $\varepsilon(NO_3^-)$ is low in both datasets, with an average of 13.5% for ANARChE and 21.3% for SEARCH. As shown in sensitivity tests, particle pH is not sensitive to the increase of NH_3 + NH_4^+ concentration under ANARChE/SEARCH conditions and the refractory ions only have a small effect on pH due to low concentrations.

The predicted concentrations and partitioning fractions of semivolatile species generally agree well with observations. For ANARChE, there is an overestimation of NH_3 (slope of 1.29) and an underestimation of NH_4^+ and $\varepsilon(NH_4^+)$. The predicted NH_3 has a better agreement with measurements for SEARCH data. The HNO_3 concentrations are reproduced by the model while the NO_3^- concentrations and $\varepsilon(NO_3^-)$ are more difficult to predict probably due to the relatively low NO_3^- level compared to HNO_3. Sensitivity tests were performed to evaluate the NH_3, HNO_3 and RH measurement uncertainties. Most of the results only show a slight change in the relationship between prediction and observation, except for NO_3^- and $\varepsilon(NO_3^-)$ when RH is increased by 10% or HNO_3 concentrations are divided by two. Using hourly averaged data did not improve the prediction.

The S curves (theoretical $\varepsilon(NH_4^+)$ and $\varepsilon(NO_3^-)$ as a function of pH) were calculated based on the average T, W_i and activity coefficients from the ANARChE data. The

observed $\varepsilon(NH_4^+)$ from a subset (average T ± 2 K and W_i ± 5 μg m^{-3}) agrees with the S curve while observed $\varepsilon(NO_3^-)$ is lower than theoretical values. The measurement uncertainties of NH_3 (±20%) and HNO_3 (perhaps double the actual level) only slightly changed the theoretical curve. S curve was then fit to the predicted $\varepsilon(NH_4^+)$ and $\varepsilon(NO_3^-)$ vs. pH data. Based on the regression equations, it is estimated that increasing pH by 1 unit (i.e. from 1.92 to 2.92) would lead to the increase of $\varepsilon(NO_3^-)$ from 12.0% to 57.6%, thus more nitrate formation is expected.

The diurnal cycles from ANARChE and SEARCH show that fine particle pH peaked in the early morning and decreased during the day, followed by an increase at night. This could be explained by its correlation with W_i which is a nonlinear function of RH. The negative correlation between RH and T led to the daytime decrease in RH and W_i, resulting in an elevated H^+ concentration in particle water. RH is higher at night and therefore H^+ is diluted by W_i. The observed $\varepsilon(NH_4^+)$ from ANARChE did not show a significant diurnal variation compared to the results from SEARCH, while $\varepsilon(NO_3^-)$ from both datasets had a good correlation with pH, suggesting that $\varepsilon(NO_3^-)$ is more sensitive to pH change than $\varepsilon(NH_4^+)$.

APPENDIX A. SENSITIVITY TESTS

As mentioned in 3.2, four cases were considered in this study to evaluate the influence of measurement uncertainties on model performance, including (1) measured NH_3 concentrations ± 20%, (2) using half HNO_3 concentrations, (3) the refractory ions were excluded, and (4) RH (0 to 1) was increased by 0.05 or 0.1.

In case 1, the NH_3 measurement uncertainties did not have a large influence on the regressions. The slope of the NH_3 regression line only decreased from 1.29 to 1.25 when NH_3 concentration was 20% higher, therefore it could not account for the overprediction of NH_3. The change in NO_3^- and $\varepsilon(NO_3^-)$ regression line slopes is due to pH variation, since the observed NO_3^- and $\varepsilon(NO_3^-)$ remained the same when perturbing NH_3 concentrations. In case 2, The NH_3-NH_4^+ concentrations and $\varepsilon(NH_4^+)$ were not significantly affected, and R^2 of the HNO_3 fit slightly decreased by 0.03. The discrepancy of NO_3^- between model prediction and observation became larger (slope decreased from 0.83 to 0.59). The scatter of $\varepsilon(NO_3^-)$ data has not improved, and the average predicted $\varepsilon(NO_3^-)$ shifted to lower value while $\varepsilon(NO_3^-)$ from measurement increased (with unchanged NO_3^- concentration and half HNO_3).

The analysis above is based on the whole dataset, while some data points (15 in total) with very low observed $\varepsilon(NH_4^+)$ and predicted $\varepsilon(NH_4^+)$ of ~50% can be seen on the left of Figure 6(c). The low observed $\varepsilon(NH_4^+)$ is unlikely to happen in Atlanta. When these points are considered outliers, the only significant difference is the $\varepsilon(NH_4^+)$ regression. Results after removing outliers are shown in Figure A-2, Figure A-4 and Figure A-6. Taking the unperturbed data as an example, the slope increased from 0.72 to 0.86 and the

intercept decreased from 1.59 to −5.65. R^2 increased from 0.55 to 0.71. The regression line is almost parallel to the 1:1 line but shifts to lower predicted $\varepsilon(NH_4^+)$ values, indicating that the discrepancy may be systematic.

The average pH decreased to 1.82 after removing data at RH > 90%, and both slopes of NO_3^- and $\varepsilon(NO_3^-)$ regression lines decreased. The other regressions were not largely affected. The $\varepsilon(NO_3^-)$ slope showed the largest decrease from 0.82 to 0.57. Removing refractory ions from calculation (case 3) did not introduce significant changes.

It was expected that increasing RH would lead to an increase of particle-phase species concentrations, thus the $\varepsilon(NH_4^+)$ regression line would shift toward the 1:1 line. As a result, after increasing RH by 10%, the average predicted $\varepsilon(NH_4^+)$ increased from 34.0% to 37.3% that is still lower than the observed value of 45.2%. Data points in Figure A-9(d) moved closer to the 1:1 line but most of them are still below that. The predicted NO_3^- and $\varepsilon(NO_3^-)$ are more sensitive to RH change. When RH was 5% higher, the slopes of NO_3^- and $\varepsilon(NO_3^-)$ regression lines increased from 0.75 to 1.04 and from 0.57 to 0.87, respectively. The overprediction became more significant when RH was increased by 10%.

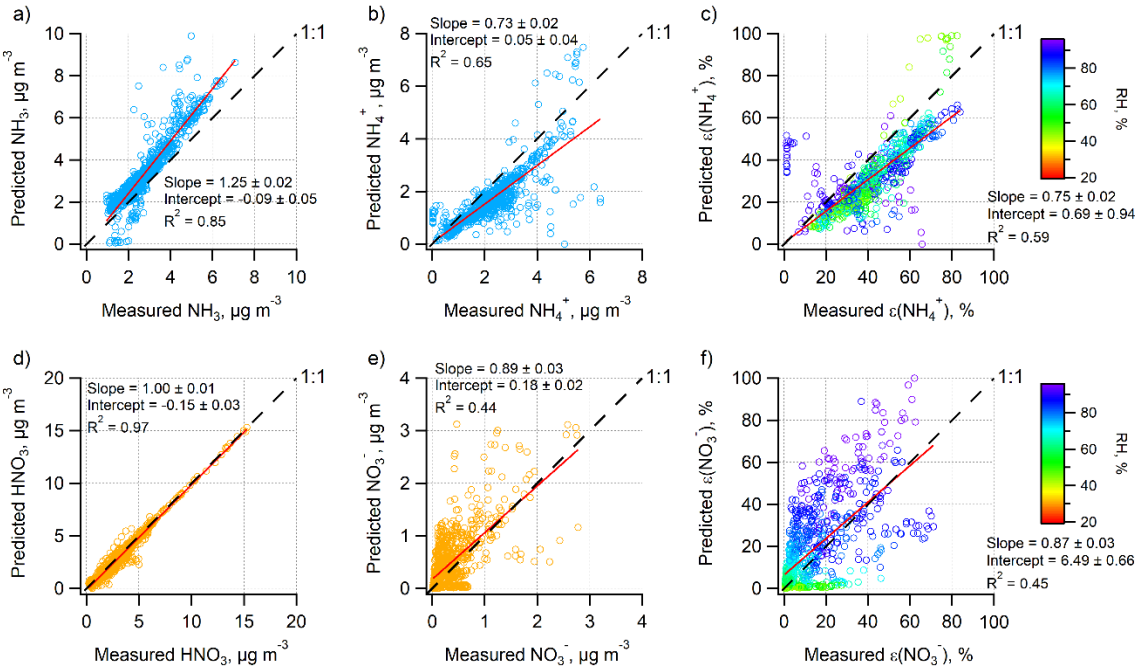

Figure A-1 Prediction vs. observation for 120% of NH_3 concentration as model input. The measured NH_3 concentration in (a) is 1.2 times the observed level.

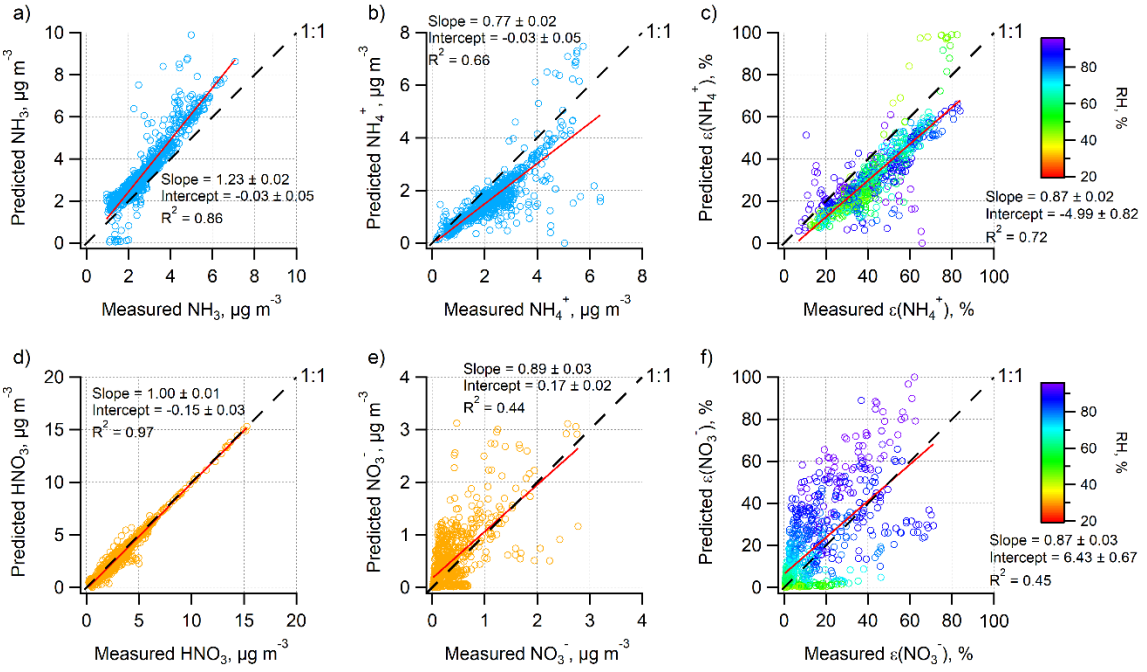

Figure A-2 Same as Figure A-1 (120% of NH_3 concentrations). The low observed $\varepsilon(NH_4^+)$ outliers are removed from each graph.

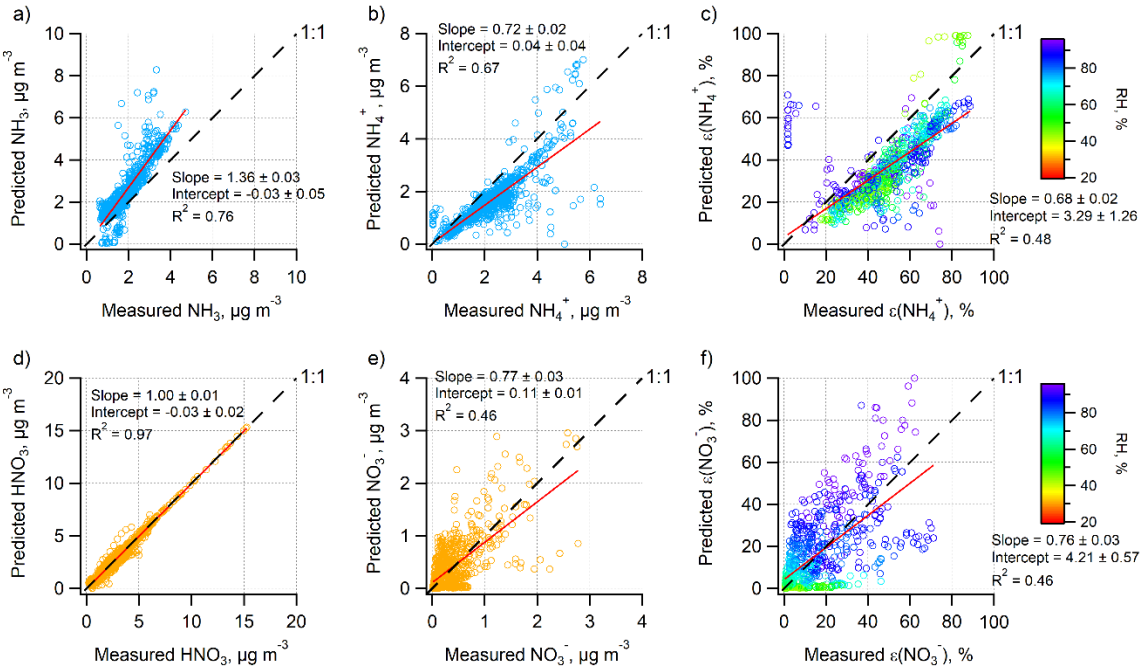

Figure A-3 Prediction vs. observation for 80% of NH_3 concentration as model input. The measured NH_3 concentration in (a) is 0.8 times the observed level.

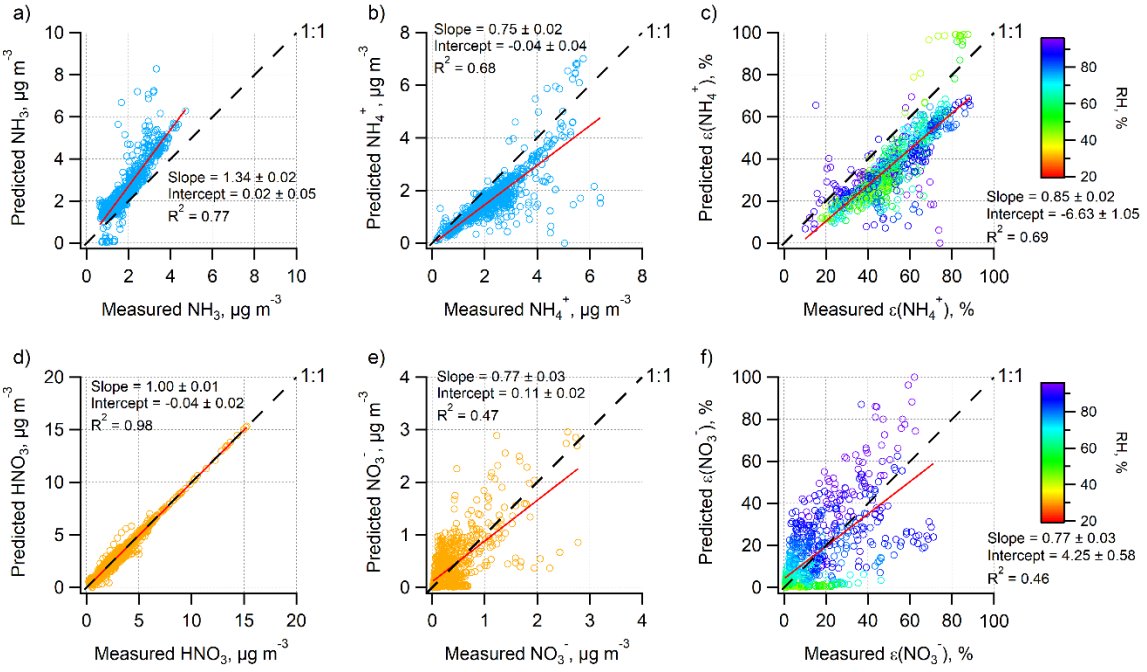

Figure A-4 Same as Figure A-3 (80% of NH_3 concentrations). The low observed $\varepsilon(NH_4^+)$ outliers are removed from each graph.

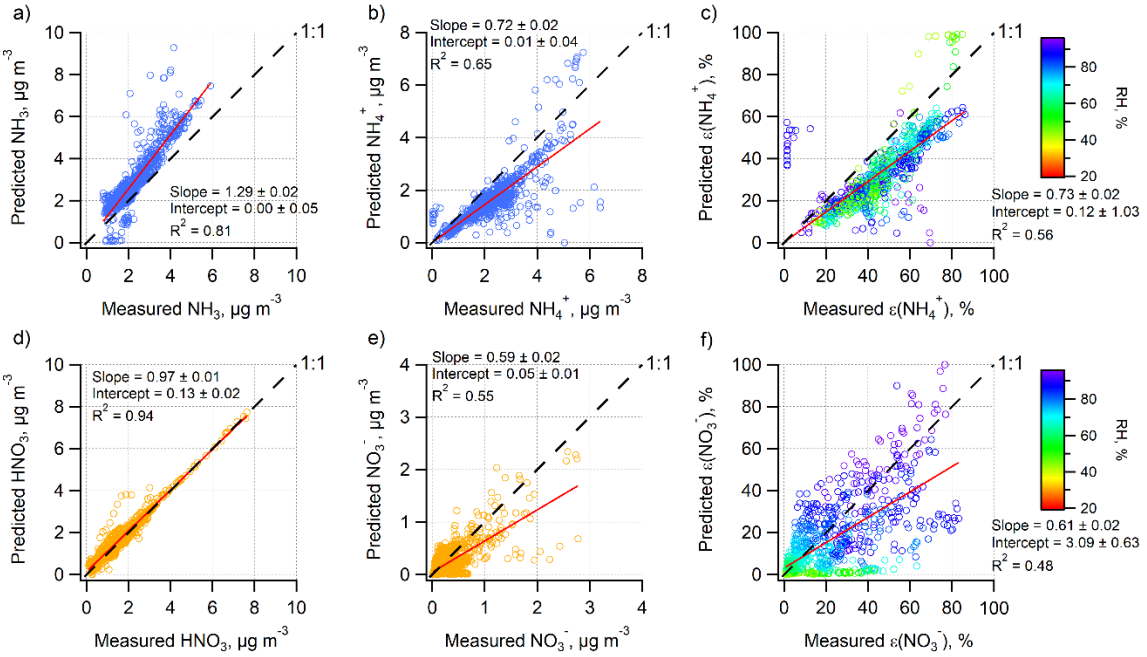

Figure A-5 Prediction vs. observation for half HNO_3 concentration as model input. The measured HNO_3 concentration in (d) is divided by 2.

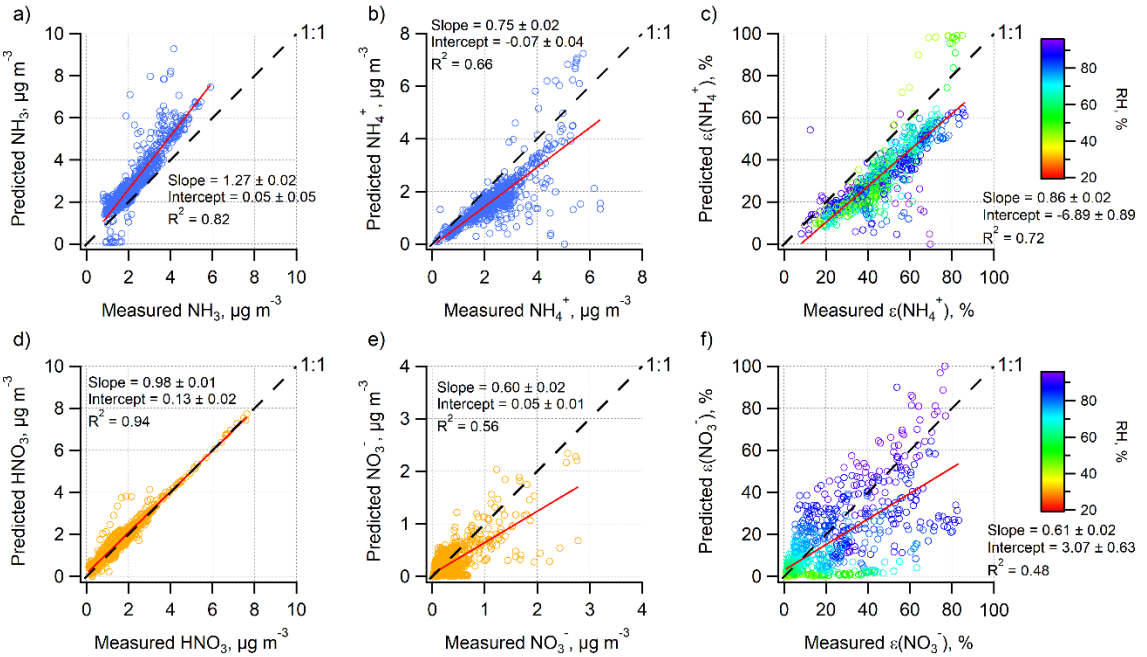

Figure A-6 Same as Figure A-5 (half HNO_3 concentrations). The low observed $\varepsilon(NH_4^+)$ outliers are removed from each graph.

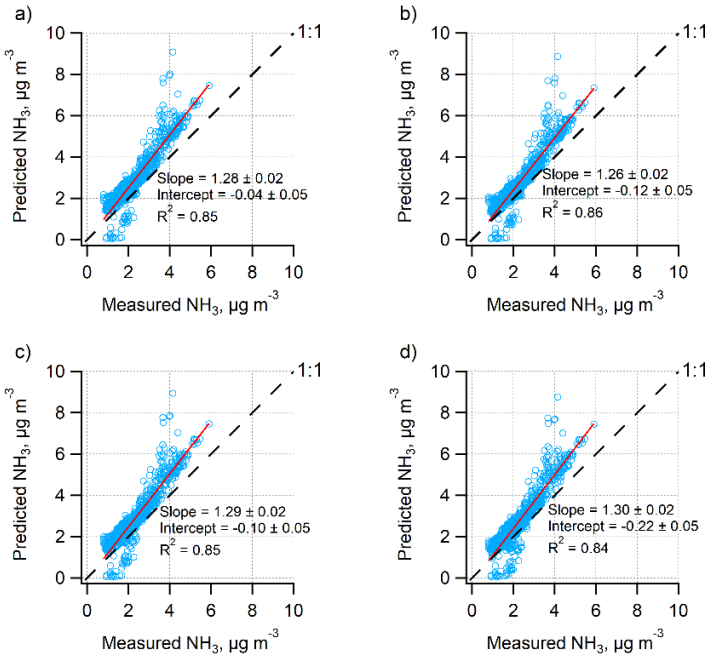

Figure A-7 Predicted vs. observed NH_3 concentrations for (a) original data with RH < 90%, (b) excluding refractory ions, (c) RH + 5%, and (d) RH + 10%.

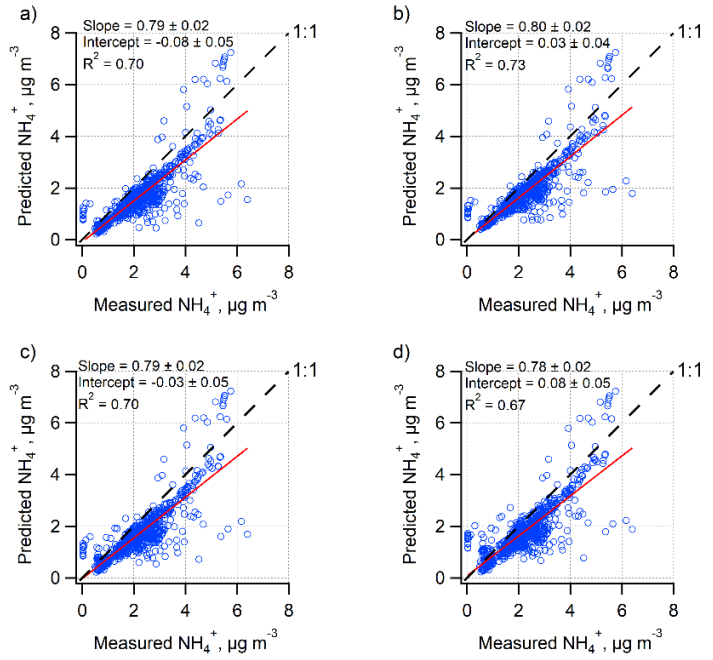

Figure A-8 Predicted vs. observed NH_4^+ concentrations for (a) original data with RH < 90%, (b) excluding refractory ions, (c) RH + 5%, and (d) RH + 10%.

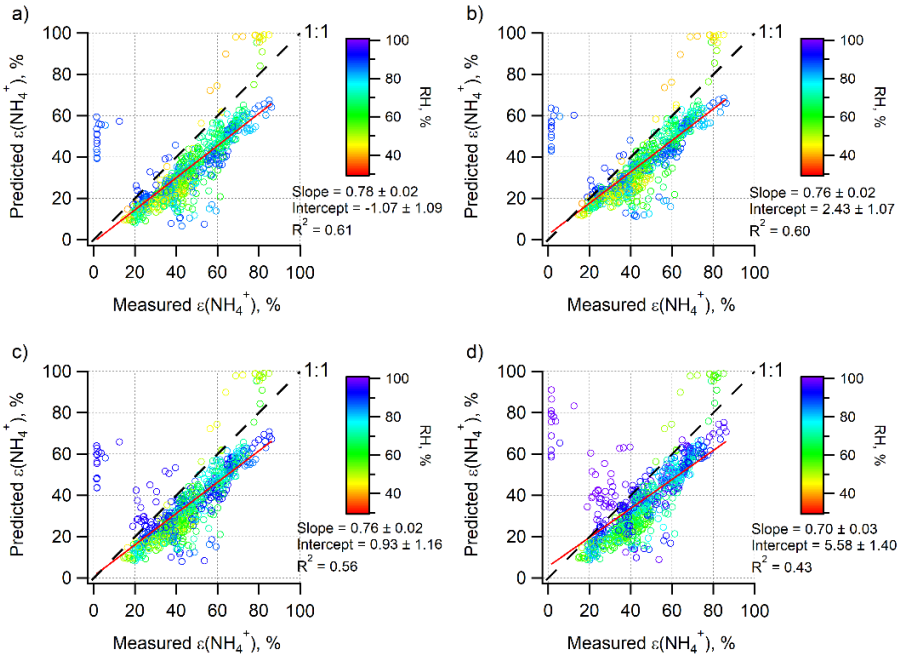

Figure A-9 Predicted vs. observed $\varepsilon(NH_4^+)$ for (a) original data with RH < 90%, (b) excluding refractory ions, (c) RH + 5%, and (d) RH + 10%.

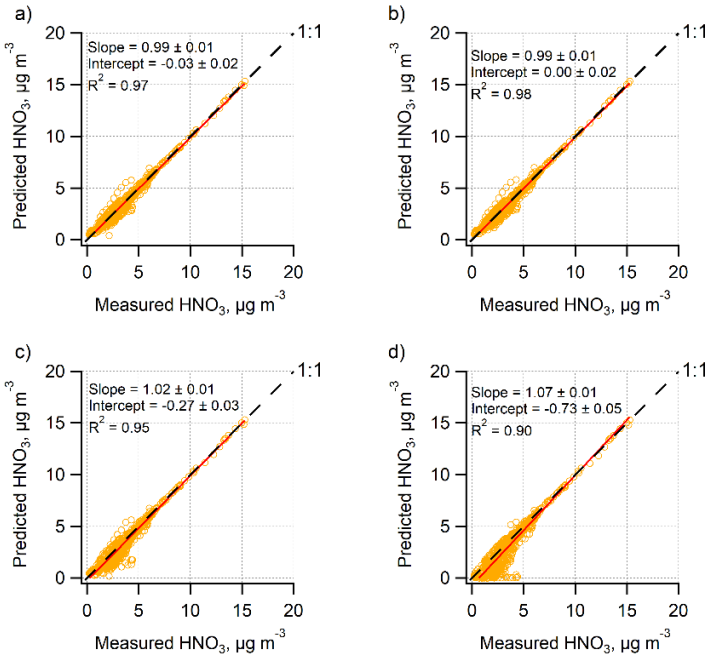

Figure A-10 Predicted vs. observed HNO_3 concentrations for (a) original data with RH < 90%, (b) excluding refractory ions, (c) RH + 5%, and (d) RH + 10%.

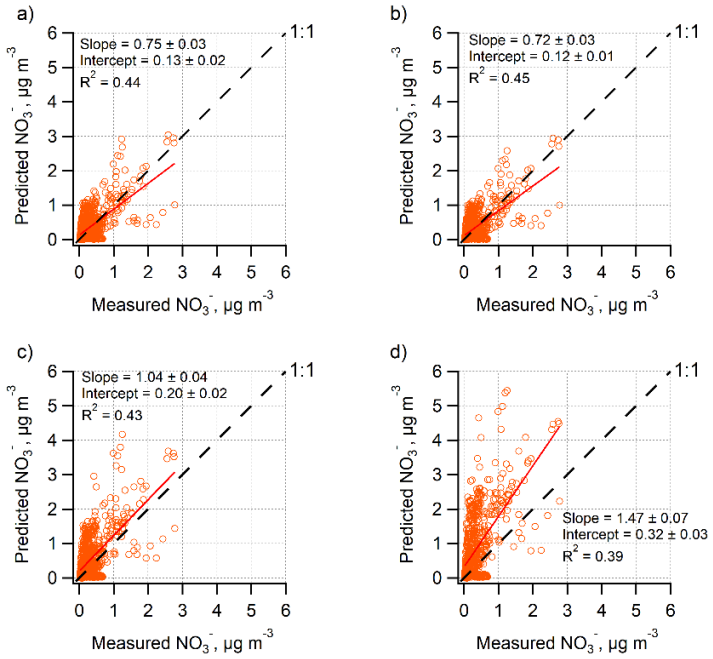

Figure A-11 Predicted vs. observed NO_3^- concentrations for (a) original data with RH < 90%, (b) excluding refractory ions, (c) RH + 5%, and (d) RH + 10%.

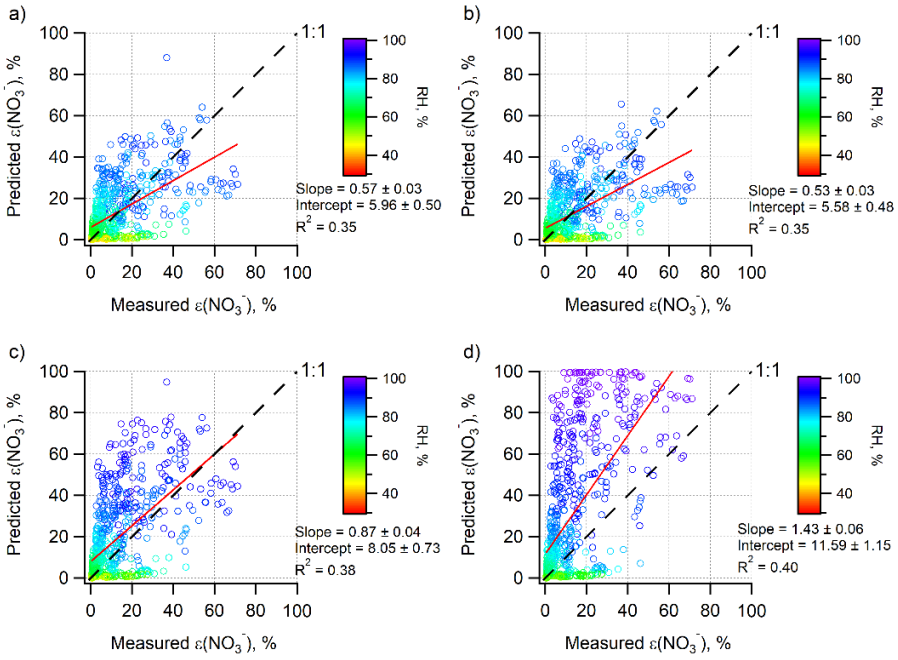

Figure A-12 Predicted vs. observed $\varepsilon(NO_3^-)$ for (a) original data with RH < 90%, (b) excluding refractory ions, (c) RH + 5%, and (d) RH + 10%.

REFERENCES

Cao, G., and Jang, M.: Effects of particle acidity and UV light on secondary organic aerosol formation from oxidation of aromatics in the absence of NO_x, Atmospheric Environment, 41, 7603-7613, 10.1016/j.atmosenv.2007.05.034, 2007.

Chameides, W. L., and Davis, D. D.: The Free Radical Chemistry of Cloud Droplets And Its Impact Upon the Composition of Rain, Journal of Geophysical Research: Oceans, 87, 4863-4877, 10.1029/JC087iC07p04863, 1982.

Cheng, Y., Zheng, G., Wei, C., Mu, Q., Zheng, B., Wang, Z., Gao, M., Zhang, Q., He, K., Carmichael, G., Pöschl, U., and Su, H.: Reactive nitrogen chemistry in aerosol water as a source of sulfate during haze events in China, Science Advances, 2, 10.1126/sciadv.1601530, 2016.

Clegg, S. L., and Brimblecombe, P.: Equilibrium Partial Pressures and Mean Activity and Osmotic Coefficients of 0-100% Nitric Acid as a Function of Temperature, The Journal of Physical Chemistry, 94, 5369-5380, 10.1021/j100376a038, 1990.

Clegg, S. L., Brimblecombe, P., and Wexler, A. S.: Thermodynamic Model of the System H^+–NH_4^+–SO_4^{2-}–NO_3^-–H_2O at Tropospheric Temperatures, The Journal of Physical Chemistry A, 102, 2137-2154, 10.1021/jp973042r, 1998.

de Gouw, J. A., Parrish, D. D., Frost, G. J., and Trainer, M.: Reduced emissions of CO_2, NOx, and SO_2 from U.S. power plants owing to switch from coal to natural gas with combined cycle technology, Earth's Future, 2, 75-82, 10.1002/2013EF000196, 2014.

Dockery, D. W., Cunningham, J., Damokosh, A. I., Neas, L. M., Spengler, J. D., Koutrakis, P., Ware, J. H., Raizenne, M., and Speizer, F. E.: Health Effects of Acid Aerosols on North American Children: Respiratory Symptoms, Environmental Health Perspectives, 104, 500-505, 10.2307/3432990, 1996.

Fountoukis, C., and Nenes, A.: ISORROPIA II: a computationally efficient thermodynamic equilibrium model for K^+–Ca^{2+}–Mg^{2+}–NH_4^+–Na^+–SO_4^{2-}–NO_3^-–Cl^-–H_2O aerosols, Atmos. Chem. Phys., 7, 4639-4659, 10.5194/acp-7-4639-2007, 2007.

Fountoukis, C., Nenes, A., Sullivan, A., Weber, R., Van Reken, T., Fischer, M., Matías, E., Moya, M., Farmer, D., and Cohen, R. C.: Thermodynamic characterization of Mexico City aerosol during MILAGRO 2006, Atmos. Chem. Phys., 9, 2141-2156, 10.5194/acp-9-2141-2009, 2009.

Friese, E., and Ebel, A.: Temperature Dependent Thermodynamic Model of the System H^+–NH_4^+–Na^+–SO_4^{2-}–NO_3^-–Cl^-–H_2O, The Journal of Physical Chemistry A, 114, 11595-11631, 10.1021/jp101041j, 2010.

Guo, H., Xu, L., Bougiatioti, A., Cerully, K. M., Capps, S. L., Hite Jr, J. R., Carlton, A. G., Lee, S. H., Bergin, M. H., Ng, N. L., Nenes, A., and Weber, R. J.: Fine-particle water and pH in the southeastern United States, Atmos. Chem. Phys., 15, 5211-5228, 10.5194/acp-15-5211-2015, 2015.

Guo, H., Sullivan, A. P., Campuzano-Jost, P., Schroder, J. C., Lopez-Hilfiker, F. D., Dibb, J. E., Jimenez, J. L., Thornton, J. A., Brown, S. S., Nenes, A., and Weber, R. J.: Fine particle pH and the partitioning of nitric acid during winter in the northeastern United States, Journal of Geophysical Research: Atmospheres, 121, 10,355-10,376, 10.1002/2016JD025311, 2016.

Guo, H., Liu, J., Froyd, K. D., Roberts, J. M., Veres, P. R., Hayes, P. L., Jimenez, J. L., Nenes, A., and Weber, R. J.: Fine particle pH and gas–particle phase partitioning of inorganic species in Pasadena, California, during the 2010 CalNex campaign, Atmos. Chem. Phys., 17, 5703-5719, 10.5194/acp-17-5703-2017, 2017a.

Guo, H., Weber, R. J., and Nenes, A.: High levels of ammonia do not raise fine particle pH sufficiently to yield nitrogen oxide-dominated sulfate production, Scientific Reports, 7, 12109, 10.1038/s41598-017-11704-0, 2017b.

Gwynn, R. C., Burnett, R. T., and Thurston, G. D.: A Time-Series Analysis of Acidic Particulate Matter and Daily Mortality and Morbidity in the Buffalo, New York, Region, Environmental Health Perspectives, 108, 125-133, 10.2307/3454510, 2000.

Hand, J. L., Schichtel, B. A., Malm, W. C., and Pitchford, M. L.: Particulate sulfate ion concentration and SO_2 emission trends in the United States from the early 1990s through 2010, Atmos. Chem. Phys., 12, 10353-10365, 10.5194/acp-12-10353-2012, 2012.

Hansen, D. A., Edgerton, E. S., Hartsell, B. E., Jansen, J. J., Kandasamy, N., Hidy, G. M., and Blanchard, C. L.: The Southeastern Aerosol Research and Characterization

Study: Part 1—Overview, Journal of the Air & Waste Management Association, 53, 1460-1471, 10.1080/10473289.2003.10466318, 2003.

Harris, E., Sinha, B., van Pinxteren, D., Tilgner, A., Fomba, K. W., Schneider, J., Roth, A., Gnauk, T., Fahlbusch, B., Mertes, S., Lee, T., Collett, J., Foley, S., Borrmann, S., Hoppe, P., and Herrmann, H.: Enhanced Role of Transition Metal Ion Catalysis During In-Cloud Oxidation of SO_2, Science, 340, 727-730, 10.1126/science.1230911, 2013.

Hennigan, C. J., Izumi, J., Sullivan, A. P., Weber, R. J., and Nenes, A.: A critical evaluation of proxy methods used to estimate the acidity of atmospheric particles, Atmos. Chem. Phys., 15, 2775-2790, 10.5194/acp-15-2775-2015, 2015.

Hidy, G. M., Blanchard, C. L., Baumann, K., Edgerton, E., Tanenbaum, S., Shaw, S., Knipping, E., Tombach, I., Jansen, J., and Walters, J.: Chemical climatology of the southeastern United States, 1999−2013, Atmos. Chem. Phys., 14, 11893-11914, 10.5194/acp-14-11893-2014, 2014.

Hoffmann, M. R., and Edwards, J. O.: Kinetics of the Oxidation of Sulfite by Hydrogen Peroxide in Acidic Solution, The Journal of Physical Chemistry, 79, 2096-2098, 10.1021/j100587a005, 1975.

Iinuma, Y., Böge, O., Gnauk, T., and Herrmann, H.: Aerosol-chamber study of the α-pinene/O_3 reaction: influence of particle acidity on aerosol yields and products, Atmospheric Environment, 38, 761-773, 10.1016/j.atmosenv.2003.10.015, 2004.

Ito, T., Nenes, A., Johnson, M. S., Meskhidze, N., and Deutsch, C.: Acceleration of oxygen decline in the tropical Pacific over the past decades by aerosol pollutants, Nature Geoscience, 9, 443-447, 10.1038/ngeo2717, 2016.

Jacob, D. J.: Chemistry of OH in Remote Clouds and Its Role in the Production of Formic Acid and Peroxymonosulfate, Journal of Geophysical Research: Atmospheres, 91, 9807-9826, 10.1029/JD091iD09p09807, 1986.

Jang, M., Czoschke, N. M., Lee, S., and Kamens, R. M.: Heterogeneous Atmospheric Aerosol Production by Acid-Catalyzed Particle-Phase Reactions, Science, 298, 814-817, 10.1126/science.1075798, 2002.

Jang, M., Cao, G., and Paul, J.: Colorimetric Particle Acidity Analysis of Secondary Organic Aerosol Coating on Submicron Acidic Aerosols, Aerosol Science and Technology, 42, 409-420, 10.1080/02786820802154861, 2008.

Li, W., Xu, L., Liu, X., Zhang, J., Lin, Y., Yao, X., Gao, H., Zhang, D., Chen, J., Wang, W., Harrison, R. M., Zhang, X., Shao, L., Fu, P., Nenes, A., and Shi, Z.: Air pollution-aerosol interactions produce more bioavailable iron for ocean ecosystems, Science Advances, 3, 10.1126/sciadv.1601749, 2017.

Liu, M., Song, Y., Zhou, T., Xu, Z., Yan, C., Zheng, M., Wu, Z., Hu, M., Wu, Y., and Zhu, T.: Fine particle pH during severe haze episodes in northern China, Geophysical Research Letters, 44, 5213-5221, 10.1002/2017GL073210, 2017.

Longo, A. F., Feng, Y., Lai, B., Landing, W. M., Shelley, R. U., Nenes, A., Mihalopoulos, N., Violaki, K., and Ingall, E. D.: Influence of Atmospheric Processes on the Solubility and Composition of Iron in Saharan Dust, Environmental Science & Technology, 50, 6912-6920, 10.1021/acs.est.6b02605, 2016.

Meskhidze, N., Chameides, W. L., Nenes, A., and Chen, G.: Iron mobilization in mineral dust: Can anthropogenic SO_2 emissions affect ocean productivity?, Geophysical Research Letters, 30, 10.1029/2003GL018035, 2003.

Moore, C. M., Mills, M. M., Arrigo, K. R., Berman-Frank, I., Bopp, L., Boyd, P. W., Galbraith, E. D., Geider, R. J., Guieu, C., Jaccard, S. L., Jickells, T. D., La Roche, J., Lenton, T. M., Mahowald, N. M., Marañón, E., Marinov, I., Moore, J. K., Nakatsuka, T., Oschlies, A., Saito, M. A., Thingstad, T. F., Tsuda, A., and Ulloa, O.: Processes and patterns of oceanic nutrient limitation, Nature Geoscience, 6, 701-710, 10.1038/ngeo1765, 2013.

Nenes, A., Pandis, S. N., and Pilinis, C.: ISORROPIA: A New Thermodynamic Equilibrium Model for Multiphase Multicomponent Inorganic Aerosols, Aquatic Geochemistry, 4, 123-152, 10.1023/A:1009604003981, 1998.

Nenes, A., Krom, M. D., Mihalopoulos, N., Van Cappellen, P., Shi, Z., Bougiatioti, A., Zarmpas, P., and Herut, B.: Atmospheric acidification of mineral aerosols: a source of bioavailable phosphorus for the oceans, Atmos. Chem. Phys., 11, 6265-6272, 10.5194/acp-11-6265-2011, 2011.

Nowak, J. B., Huey, L. G., Russell, A. G., Tian, D., Neuman, J. A., Orsini, D., Sjostedt, S. J., Sullivan, A. P., Tanner, D. J., Weber, R. J., Nenes, A., Edgerton, E., and

Fehsenfeld, F. C.: Analysis of urban gas phase ammonia measurements from the 2002 Atlanta Aerosol Nucleation and Real-Time Characterization Experiment (ANARChE), Journal of Geophysical Research: Atmospheres, 111, D17308, 10.1029/2006JD007113, 2006.

Orsini, D. A., Ma, Y., Sullivan, A., Sierau, B., Baumann, K., and Weber, R. J.: Refinements to the particle-into-liquid sampler (PILS) for ground and airborne measurements of water soluble aerosol composition, Atmospheric Environment, 37, 1243-1259, 10.1016/S1352-2310(02)01015-4, 2003.

Penkett, S. A., Jones, B. M. R., Brich, K. A., and Eggleton, A. E. J.: The importance of atmospheric ozone and hydrogen peroxide in oxidising sulphur dioxide in cloud and rainwater, Atmospheric Environment, 13, 123-137, 10.1016/0004-6981(79)90251-8, 1979.

Saylor, R. D., Edgerton, E. S., Hartsell, B. E., Baumann, K., and Hansen, D. A.: Continuous gaseous and total ammonia measurements from the southeastern aerosol research and characterization (SEARCH) study, Atmospheric Environment, 44, 4994-5004, 10.1016/j.atmosenv.2010.07.055, 2010.

Seinfeld, J. H., and Pandis, S. N.: Atmospheric Chemistry and Physics: from Air Pollution to Climate Change, 3rd ed., John Wiley & Sons, Inc., Hoboken, New Jersey, 2016.

Srivastava, R. K., Jozewicz, W., and Singer, C.: SO_2 Scrubbing Technologies: A Review, Environmental Progress, 20, 219-228, 10.1002/ep.670200410, 2001.

Stockdale, A., Krom, M. D., Mortimer, R. J. G., Benning, L. G., Carslaw, K. S., Herbert, R. J., Shi, Z., Myriokefalitakis, S., Kanakidou, M., and Nenes, A.: Understanding the nature of atmospheric acid processing of mineral dusts in supplying bioavailable phosphorus to the oceans, Proceedings of the National Academy of Sciences, 113, 14639-14644, 10.1073/pnas.1608136113, 2016.

Stumm, W., and Morgan, J. J.: Aquatic Chemistry : Chemical Equilibria and Rates in Natural Waters, 3rd ed., John Wiley & Sons, Inc., 1996.

Surratt, J. D., Chan, A. W. H., Eddingsaas, N. C., Chan, M., Loza, C. L., Kwan, A. J., Hersey, S. P., Flagan, R. C., Wennberg, P. O., and Seinfeld, J. H.: Reactive intermediates revealed in secondary organic aerosol formation from isoprene, Proceedings of the National Academy of Sciences, 107, 6640-6645, 10.1073/pnas.0911114107, 2010.

U.S. Environmental Protection Agency: Air Pollutant Emissions Trends Data, https://www.epa.gov/air-emissions-inventories/air-pollutant-emissions-trends-data (last access: 25 April 2018), 2017.

Weber, R. J., Orsini, D., Daun, Y., Lee, Y. N., Klotz, P. J., and Brechtel, F.: A Particle-into-Liquid Collector for Rapid Measurement of Aerosol Bulk Chemical Composition, Aerosol Science and Technology, 35, 718-727, 10.1080/02786820152546761, 2001.

Weber, R. J., Guo, H., Russell, A. G., and Nenes, A.: High aerosol acidity despite declining atmospheric sulfate concentrations over the past 15 years, Nature Geoscience, 9, 282-285, 10.1038/ngeo2665, 2016.

Xu, L., Middlebrook, A. M., Liao, J., de Gouw, J. A., Guo, H., Weber, R. J., Nenes, A., Lopez-Hilfiker, F. D., Lee, B. H., Thornton, J. A., Brock, C. A., Neuman, J. A., Nowak, J. B., Pollack, I. B., Welti, A., Graus, M., Warneke, C., and Ng, N. L.: Enhanced formation of isoprene-derived organic aerosol in sulfur-rich power plant plumes during Southeast Nexus, Journal of Geophysical Research: Atmospheres, 121, 11,137-11,153, 10.1002/2016JD025156, 2016.

Zhang, Q., Jimenez, J. L., Worsnop, D. R., and Canagaratna, M.: A Case Study of Urban Particle Acidity and Its Influence on Secondary Organic Aerosol, Environmental Science & Technology, 41, 3213-3219, 10.1021/es061812j, 2007.